J. Fluid Mech. (1991), *vol.* 233, *pp.* 211–242
Printed in Great Britain

Reaction in a scalar mixing layer

By R. W. BILGER, L. R. SAETRAN† AND L. V. KRISHNAMOORTHY
Department of Mechanical Engineering, University of Sydney, NSW 2006, Australia

(Received 18 July 1990 and in revised form 21 May 1991)

Reaction in a scalar mixing layer in grid-generated turbulence is studied experimentally by doping half of the flow with nitric oxide and the other half with ozone. The flow conditions and concentrations are such that the chemical reaction is passive and the flow and chemical timescales are of the same order. Conserved scalar theory for such flows is outlined and further developed; it is used as a basis for presentation of the experimental results. Continuous measurements of concentration are limited in their spatial and temporal resolution but capture sufficient of their spectra for adequate second-order correlations to be made. Two components of velocity have been measured simultaneously with hot-wire anemometry. Conserved scalar mixing results, deduced from reacting and non-reacting measurements of concentration, show the independence of concentration level and concentration ratio expected for passive reacting flow. The results are subject to several limitations due to the necessary experimental compromises, but they agree generally with measurements made in thermal mixing layers. Reactive scalar statistics are consistent with the realizability constraints obtainable from conserved scalar theory where such constraints apply, and otherwise are generally found to lie between the conserved scalar theory limits for frozen and very fast chemistry. It is suggested that Toor's (1969) closure for the mean chemical reaction rate could be improved by interpolating between the frozen and equilibrium values for the covariance. The turbulent fluxes of the reactive scalars are found to approximately obey the gradient model but the value of the diffusivity is found to depend on the Damköhler number.

1. Introduction

The turbulent flow behind a grid, which has at some upstream location a step change in temperature in the direction transverse to the mean flow direction, has been termed the thermal mixing layer. It has been studied experimentally by Watt & Baines (1973), Keffer, Olsen & Kawall (1977), LaRue & Libby (1981), LaRue, Libby & Seshadri (1981), Ma & Warhaft (1986) and Gibson, Jones & Kanellopoulos (1989), and theoretically by Libby (1975), Durbin (1980), Wu & O'Brien (1982), Lumley (1986) and Gibson *et al.* (1989). Durbin's stochastic model is presented in terms of species concentrations, but since heat and species are transported in a similar fashion in a turbulent flow at low Mach number the problem is analogous. We can speak in general terms of a scalar mixing layer. For small temperature differences and dilute species, variations in the fluid density and viscosity will be small and the effect of the scalars on the flow can be negligible. The scalars are then said to be passive. Study of the passive scalar mixing layer will help to elucidate many aspects

† Present address: Division of Hydro and Gas Dynamics, NTH, University of Trondheim, Norway.

of turbulent mixing. Here we address the effects of chemical reaction. Hsieh & O'Brien (1986) give modelling results for low rates of reaction.

The study of turbulent reacting flows is important in many engineering, geophysical and biological contexts, e.g. combustion chambers for engines and furnaces; chemical reactors; dispersion in the atmosphere, oceans, lakes and rivers; and biological processes in aquatic environments. Turbulent mixing processes lead to large fluctuations in scalar quantities such as temperature and species concentrations. Rates of reaction are usually nonlinear functions of these scalar quantities and their mean rates of reaction are not simply expressible in terms of the mean values of the scalars (Toor 1969; Donaldson & Hilst 1972). Scalar correlations play a significant role. The turbulence can thus significantly affect the rates of reaction. Indeed it is found for fast reactions that the rate of reaction is controlled by the rate of mixing produced by the turbulence. Reaction may also affect turbulent transport. Models for turbulent transport, such as the gradient transport model, which are found to be useful for non-reactive scalars, can be significantly altered for reactive scalars. It has been found (Moss 1980) that transport up the mean gradient, rather than down the mean gradient can occur. Libby & Bray (1981) attribute such 'countergradient' transport to dynamical processes associated with density fluctuations and mean pressure gradients. Effects are possible in passive reacting flow (Seinfeld 1975; Lamb 1976) and need clarification. Hill (1976), Libby & Williams (1980) and Bilger (1989) are useful entries into the literature on turbulent reacting flows.

We study here the reaction between two chemical species A and B which are initially in separate streams, that is they are non-premixed. Of particular interest is the effect of the relative rates of chemical reaction and mixing (expressible in terms of a Damköhler number, N_D) on the reactive species statistics (means, variance, covariances, etc.), the mean chemical rate, and the modelling of scalar transport. The reactants are assumed to undergo a second-order irreversible reaction. The concentrations of the reactants in the inlet streams is assumed to be spatially uniform and constant in time. The theory for such two-stream mixing problems with chemical reaction and turbulent flow is well developed for the special case of equal molecular diffusivities for all the scalars. Limiting cases of fast chemistry ($N_D \to \infty$) and slow chemistry ($N_D \to 0$) are identified and have solutions expressible in terms of the statistics of non-reactive scalars in the flow. For finite Damköhler number results are obtained which limit the range of reactive scalar statistical quantities. The theory makes use of linear combinations of the reactive scalars which are defined such that they have no chemical source term. Results for this 'conserved scalar' theory are briefly derived and presented here as a basis for discussion of the experimental results. In general they are applicable to all two-stream mixing problems and do not involve modelling assumptions.

Experiments have been carried out in a large slowly moving turbulent grid flow using the reaction between nitric oxide and ozone which are mixed at parts per million (p.p.m.) levels in air. The experimental conditions are such that the Damköhler number can be varied around values of the order of unity so that the rates of mixing and chemical reaction are comparable. The aim has been to get measurements of the reactant species which are sufficiently resolved spatially and temporally so that errors in their statistics will not be large. Although the diffusivities of the nitric oxide and ozone are not identical it is surmised that differential diffusion effects may not be large at moderate to high Reynolds numbers so that comparison with the conserved scalar theory may be useful. The measurements have been made in the near-field region of the grid flow, 12–21 mesh

widths downstream from the grid. Furthermore, the overall width of the flow is only 8 mesh widths, four per side, thus stretching the notation of grid turbulence to an extreme. The turbulence in this region is not fully developed. The design of the experiment represents a compromise between the desire for high Reynolds numbers, large distance downstream, Damköhler numbers in the range near unity, degree of spatial resolution and cost of construction and operation. Currently, no better source of experimental data exists and the results obtained appear to be basically valid. The measurements include two channels of hot-wire anemometry so that correlations with reactive species are obtained yielding the turbulent fluxes directly. Saetran *et al.* (1989) have presented some of the results for the first and second moments of the scalars. These are included here for completeness and to correct an error in figure 7 of that article.

2. Conserved scalar theory

A schematic of the reactive scalar mixing layer is shown in figure 1. Stream 1 contains reactant A at the uniform and constant composition Γ_{A_1} and zero of reactant B. Stream 2 contains reactant B at the uniform and constant composition Γ_{B_2} and zero of reactant A. This is a two-stream mixing problem with reaction. Conserved scalar theory for such problems is quite well developed in the literature (see e.g. Lin & O'Brien 1974; Bilger 1976*a*, Libby & Williams 1980). We recapitulate the development of the theory here, partly for completeness and ready accessibility of the results, but also to introduce some new findings.

All species are assumed dilute so that the density and other fluid properties are constant throughout the flow and the diffusion of the species is assumed to be Fickian with equal diffusivities so that they obey the conservation equation

$$\mathscr{L}(\Gamma_i) \equiv \frac{\partial \Gamma_i}{\partial t} + \boldsymbol{U}\cdot\boldsymbol{\nabla}\Gamma_i - \boldsymbol{\nabla}\cdot(\mathscr{D}\boldsymbol{\nabla}\Gamma_i) = w_i. \tag{1}$$

Here $\Gamma_i = \Gamma_i(\boldsymbol{x}, t)$ is the mole fraction of species i, w_i its reaction rate per unit total moles, $\mathscr{D}$ the molecular diffusivity, $\boldsymbol{U}$ the velocity vector, t time and $\boldsymbol{\nabla}$ the spatial derivative operator. The species A and B are assumed to undergo an irreversible second-order chemical reaction to form the product P, the stoichiometric coefficients being here assumed (without loss of generality) to be unity:

$$A + B \rightarrow P,$$

so that

$$w_A = w_B = -w_P = -k\Gamma_A\Gamma_B. \tag{2}$$

Conserved scalars $\beta^{(j)}(\boldsymbol{x}, t)$ may be defined such that they have zero chemical source term, e.g.

$$\beta' \equiv \Gamma_A - \Gamma_B; \quad \beta'' \equiv \Gamma_A + \Gamma_P; \quad \beta''' \equiv \Gamma_B + \Gamma_P. \tag{3}$$

Such conserved scalars obey the conservation equation

$$\mathscr{L}(\beta^{(j)}) = 0, \tag{4}$$

where $\mathscr{L}$ is the operator defined by the left-hand side of (1). This is the conservation equation that applies to non-reactive flow and to non-reactive species in a reactive flow. It also applies to temperature in low-Mach-number flows with negligible heat release. Dropping the identifying superscript (j) for clarity we have for all such conserved and non-reactive scalars with similar boundary conditions

$$\mathscr{L}(\hat{\beta}) = 0, \tag{5}$$

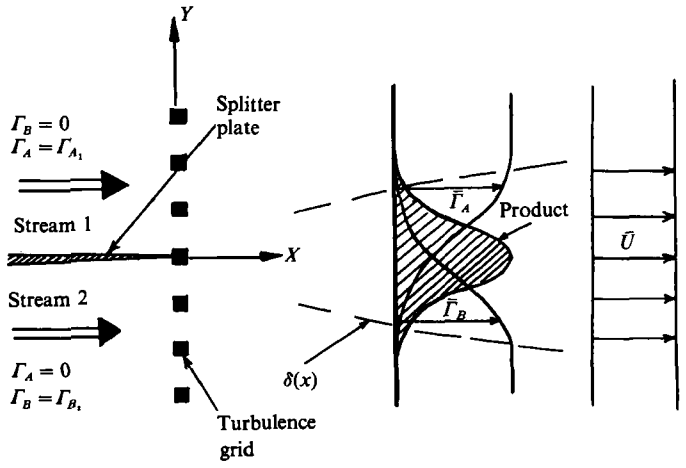

FIGURE 1. Schematic diagram of the reactive-scalar mixing layer.

with $\hat{\beta} = 1$ in stream 1, $\hat{\beta} = 0$ in stream 2,

where
$$\hat{\beta} \equiv (\beta - \beta_2)/(\beta_1 - \beta_2). \tag{6}$$

It follows (Lin & O'Brien 1974; Bilger 1976*b*) that all the $\hat{\beta}$ must be identical so that

$$\hat{\beta}(\boldsymbol{x}, t) = F(\boldsymbol{x}, t) \tag{7}$$

and F is called the mixture fraction. It has limits of 0 and 1, its values in streams 2 and 1 respectively. Since the scalars are passive the statistics of $\hat{\beta}$ and hence of F are the same in all realizations of the flow, with or without any particular reactant, they will be the same as that for temperature in a thermal mixing layer, assuming that the thermal diffusivity is equal to the species diffusivity and the boundary conditions are the same.

We have from β' in (3), and (6) and (7)

$$\Gamma_A - \Gamma_B = F(\Gamma_{A_1} + \Gamma_{B_2}) - \Gamma_{B_2}, \tag{8a}$$

$$\Gamma_A + \Gamma_P = F\Gamma_{A_1}, \tag{8b}$$

$$\Gamma_B + \Gamma_P = (1-F)\,\Gamma_{B_2}. \tag{8c}$$

These results apply for all Damköhler numbers. Using the grid mesh width M and the mean velocity $\bar{U}$ to non-dimensionalize (1) we have

$$\hat{\mathscr{L}}(\hat{\Gamma}_A) = -N_{\mathrm{D}}\,\psi\hat{\Gamma}_A\hat{\Gamma}_B, \tag{9a}$$

$$\hat{\mathscr{L}}(\hat{\Gamma}_B) = -N_{\mathrm{D}}(1-\psi)\,\hat{\Gamma}_A\hat{\Gamma}_B, \tag{9b}$$

where $\hat{\Gamma}_A \equiv \dfrac{\Gamma_A}{\Gamma_{A_1}}$, $\hat{\Gamma}_B \equiv \dfrac{\Gamma_B}{\Gamma_{B_2}}$, $\hat{\mathscr{L}}(\cdot) \equiv \dfrac{\partial}{\partial \hat{t}}(\cdot) + \hat{\boldsymbol{U}}\cdot\hat{\boldsymbol{\nabla}}(\cdot) - Pe^{-1}\nabla^2(\cdot)$, $Pe \equiv \dfrac{\bar{U}M}{\mathscr{D}}$,

$$N_{\mathrm{D}} \equiv \frac{kM(\Gamma_{A_1} + \Gamma_{B_2})}{\bar{U}}, \tag{10}$$

$$\psi \equiv \frac{\Gamma_{B_2}}{\Gamma_{A_1} + \Gamma_{B_2}}. \tag{11}$$

This definition for the Damköhler number, N_D, will give values which are low compared with definitions based on the advective timescale ($x/\bar{U}$) or the turbulence timescale ($\approx M/u'$), where u' is the r.m.s. axial velocity fluctuation of the streamwise velocity.

It is seen that for $N_D \to 0$, (9*a*, *b*) become

$$\hat{\mathscr{L}}(\hat{\Gamma}_A) = 0, \quad \hat{\mathscr{L}}(\hat{\Gamma}_B) = 0,$$

with solutions linearly related to that of F yielding

$$\lim_{N_D \to 0} \Gamma_A = \Gamma_A^0 = F\Gamma_{A_1}, \quad \lim_{N_D \to 0} \Gamma_B = \Gamma_B^0 = (1-F)\Gamma_{B_2}. \tag{12a, b}$$

These are the so-called frozen flow limits. It can be seen that (12*a*) is also obtained when $\psi = 0$, i.e. when $\Gamma_{B_2} = 0$, and (12*b*) is also obtained when $\psi = 1$, i.e. when $\Gamma_{A_1} = 0$. When $N_D \to \infty$, for finiteness of the right-hand side of (9) we must have

$$\hat{\Gamma}_A \hat{\Gamma}_B = 0,$$

which implies that either $\Gamma_A = 0$ or $\Gamma_B = 0$ or both are zero together. With the constraint of (8) this yields the so-called equilibrium flow limits to the solution

$$\lim_{N_D \to \infty} \Gamma_A = \Gamma_A^e = (\Gamma_{A_1} + \Gamma_{B_2})(F - F_s) H(F - F_s), \tag{13a}$$

$$\lim_{N_D \to \infty} \Gamma_B = \Gamma_B^e = (\Gamma_{A_1} + \Gamma_{B_2})(F_s - F) H(F_s - F), \tag{13b}$$

where $H(z)$ is the Heaviside unit step function with value zero for $z < 0$ and value unity for $z > 0$. The stoichiometric value of the mixture fraction, F_s, is given by setting both Γ_A and Γ_B equal to zero in (8):

$$F_s = \Gamma_{B_2}/(\Gamma_{A_1} + \Gamma_{B_2}) = \psi. \tag{14}$$

The frozen and equilibrium limits are bounds for finite Damköhler number

$$\Gamma_A^0 \geqslant \Gamma_A \geqslant \Gamma_A^e, \quad \Gamma_B^0 \geqslant \Gamma_B \geqslant \Gamma_B^e. \tag{15}$$

This can be proved by using (8), (12), (13) and (14) to show that

$$\Gamma_A^0 - \Gamma_A = \Gamma_B^0 - \Gamma_B = \Gamma_P,$$

and

$$\Gamma_A - \Gamma_A^e = \Gamma_B - \Gamma_B^e = \Gamma_A H(F_s - F) + \Gamma_B H(F - F_s)$$

and noting that no mole fraction can be negative. These represent a constraint on experimental measurements the violation of which must be explained in terms of differential diffusion or experimental error.

The probability density function of F, $p_F(F)$, is defined for every point in the flow (or every point and time in an ensemble of non-stationary flows) such that $p_F(F; \boldsymbol{x})\,\mathrm{d}F$ is the probability that F lies between F and $F + \mathrm{d}F$ at $\boldsymbol{x}$. We have

$$\int_0^1 p_F(F)\,\mathrm{d}F = 1 \tag{16}$$

since the domain of F is $0 \leqslant F \leqslant 1$. Since the frozen flow and equilibrium flow limits

of Γ_A and Γ_B are functions of F their statistical properties may be determined in terms of F:

$$\overline{\Gamma_A^0} = \int_0^1 \Gamma_A^0(F)\, p_F(F)\, \mathrm{d}F = \Gamma_{A_1}\bar{F}, \tag{17a}$$

$$\overline{\Gamma_B^0} = \Gamma_{B_2}(1-\bar{F}), \tag{17b}$$

$$\overline{\Gamma_A^e} = (\Gamma_{A_1}+\Gamma_{B_2})\int_{F_s}^1 (F-F_s)\, p_F(F)\, \mathrm{d}F = (\Gamma_{A_1}+\Gamma_{B_2})\{(\bar{F}-F_s)\, H(\bar{F}-F_s)+J_1 f'\}, \tag{18a}$$

$$\overline{\Gamma_B^e} = (\Gamma_{A_1}+\Gamma_{B_2})\int_0^{F_s} (F_s-F)\, p_F(F)\, \mathrm{d}F = (\Gamma_{A_1}+\Gamma_{B_2})\{(F_s-\bar{F})\, H(F_s-\bar{F})+J_1 f'\}, \tag{18b}$$

where

$$J_1 \equiv \frac{1}{2f'}\left[\int_0^1 |F-F_s|\, p_F(F)\, \mathrm{d}F - |\bar{F}-F_s|\right], \tag{18c}$$

and f' is the r.m.s. fluctuation of F. The first terms in (18a) and (18b) are $\Gamma_A^e(\bar{F})$ and $\Gamma_B^e(\bar{F})$ respectively. The integral J_1 is non-negative and an upper bound on it can be derived by noting that for any fluctuating variable Q, $\bar{Q} < (\overline{Q^2})^{\frac{1}{2}}$ and setting $Q = |F-F_s|$. This yields

$$0 < J_1 < \tfrac{1}{2}[\{1+(\bar{F}-F_s)^2/f'^2\}^{\frac{1}{2}} - |\bar{F}-F_s|/f']. \tag{19a}$$

This upper bound has a maximum of 0.5 at $\bar{F} = F_s$. Bilger (1980) shows values of J_1 for a variety of p.d.f. forms and Mudford & Bilger (1985) give an empirical correlation,

$$J_1 \approx 0.45 \exp\{-|\bar{F}-F_s|/f'\}. \tag{19b}$$

It should be noted that the only assumption behind the constraint of (19a) is that of equal species diffusivities and it will apply no matter what is the structure of the turbulence. For all degrees of reactedness of the mixture we have from (8) that

$$\bar{\Gamma}_A - \bar{\Gamma}_B = \overline{\Gamma_A^0} - \overline{\Gamma_B^0} = \overline{\Gamma_A^e} - \overline{\Gamma_B^e} = (\Gamma_{A_1}+\Gamma_{B_2})\,\bar{F} - \Gamma_{B_2}. \tag{20}$$

Denoting fluctuations from the mean by γ_A and γ_B, and their r.m.s. fluctuation by γ'_A and γ'_B, we have

$$\gamma_A^{0'}/\Gamma_{A_1} = \gamma_B^{0'}/\Gamma_{B_2} = f', \tag{21}$$

$$\overline{\gamma_A^0 \gamma_B^0} = -\Gamma_{A_1}\Gamma_{B_2} f'^2, \tag{22}$$

so that

$$\alpha^0 \equiv \overline{\gamma_A^0 \gamma_B^0}/(\overline{\Gamma_A^0}\,\overline{\Gamma_B^0}) = -f'^2/\bar{F}(1-\bar{F}) \tag{23}$$

and

$$R_{AB}^0 \equiv \overline{\gamma_A^0 \gamma_B^0}/(\gamma_A^{0'}\gamma_B^{0'}) = -1. \tag{24}$$

For the equilibrium flow limit

$$\gamma_A^{e'} = (\Gamma_{A_1}+\Gamma_{B_2})\left\{\int_{F_s}^1 (F-F_s)^2\, p_F(F)\, \mathrm{d}F - \left[\int_{F_s}^1 (F-F_s)\, p_F(F)\, \mathrm{d}F\right]^2\right\}^{\frac{1}{2}}, \tag{25a}$$

$$\gamma_B^{e'} = (\Gamma_{A_1}+\Gamma_{B_2})\left\{\int_0^{F_s} (F_s-F)^2\, p_F(F)\, \mathrm{d}F - \left[\int_0^{F_s} (F_s-F)\, p_F(F)\, \mathrm{d}F\right]^2\right\}^{\frac{1}{2}}, \tag{25b}$$

$$\overline{\gamma_A^e \gamma_B^e} = -\overline{\Gamma_A^e}\,\overline{\Gamma_B^e} = -(\Gamma_{A_1}+\Gamma_{B_2})^2\{J_1 f'|\bar{F}-F_s| + J_1^2 f'^2\}, \tag{26a}$$

$$\alpha^e \equiv \overline{\gamma_A^e \gamma_B^e}/(\overline{\Gamma_A^e}\,\overline{\Gamma_B^e}) = -1, \tag{26b}$$

$$R_{AB}^e \equiv \frac{\overline{\gamma_A^e \gamma_B^e}}{\gamma_A^{e'}\gamma_B^{e'}} = -\frac{\overline{\Gamma_A^e}\,\overline{\Gamma_B^e}}{\gamma_A^{e'}\gamma_B^{e'}}. \tag{27}$$

For all Damköhler numbers we have the constraint

$$-\overline{\gamma_A \gamma_B} < \tfrac{1}{2}(\gamma_A - \gamma_B)^2 = \tfrac{1}{2}(\Gamma_{A_1} + \Gamma_{B_2})^2 f'^2. \tag{28}$$

The mean reaction rate, $\overline{\hat{w}}$, here normalized by the chemical timescale, is defined

$$\overline{\hat{w}} = \frac{-\overline{w}_A}{k\Gamma_{A_1}\Gamma_{B_2}} = \frac{\overline{\Gamma_A \Gamma_B}}{\Gamma_{A_1}\Gamma_{B_2}}. \tag{29}$$

Normalization by the flow timescale as in (4) yields essentially $N_D \overline{\hat{w}}$. From (17) and (22) we have at the frozen flow limit

$$\overline{\hat{w}}^0 = \bar{F}(1-\bar{F}) - f'^2. \tag{30}$$

At the equilibrium limit the result from (26) for $N_D \overline{\hat{w}}$ is indeterminate. The reaction rate is then mixing controlled and may be determined (Bilger 1976*a*) by substituting (13) into (1):

$$w_A^e = \mathscr{L}(\Gamma_A^e) = \frac{\mathrm{d}\Gamma_A^e}{\mathrm{d}F}\mathscr{L}(F) - \mathscr{D}\nabla F\cdot\nabla F\frac{\mathrm{d}^2\Gamma_A^e}{\mathrm{d}F^2}$$

$$= -\mathscr{D}\nabla F\cdot\nabla F\frac{\mathrm{d}^2\Gamma_A^e}{\mathrm{d}F^2} \tag{31}$$

$$= -\mathscr{D}(\Gamma_{A_1}+\Gamma_{B_2})\nabla F\cdot\nabla F[2\delta(F-F_s)+(F-F_s)\delta'(F-F_s)]. \tag{32}$$

Here $\delta(z)$ is the Dirac delta function centred at $z = 0$ with the property that

$$\int_{-\infty}^{z}\delta(z)\,\mathrm{d}z = H(z)$$

and $\delta'(z)$ is the first derivative of $\delta(z)$ with respect to z. It is seen that the instantaneous reaction rate is confined to thin sheets at the stoichiometric isopleth surfaces given by $F(\boldsymbol{x}, t) = F_s$. Its value is thus a function of F and $\nabla F\cdot\nabla F$ and this may be averaged to yield

$$\overline{w_A^e} = \overline{w_B^e} = -\{\mathscr{D}(\nabla\bar{F}\cdot\nabla\bar{F}) + \tfrac{1}{2}\overline{\chi}_s\}(\Gamma_{A_1}+\Gamma_{B_2})\,p_F(F_s;\boldsymbol{x}). \tag{33}$$

Here

$$\overline{\chi}_s = \left\{\int_{-\infty}^{\infty}\chi p_{\chi F}(\chi, F;\boldsymbol{x})\,\delta(F-F_s)\,\mathrm{d}\chi\right\}/p_F(F_s;\boldsymbol{x}) \tag{34}$$

is the conditional expectation of χ for $F = F_s$, where

$$\chi \equiv 2\mathscr{D}\nabla f\cdot\nabla f. \tag{35}$$

Its mean, $\overline{\chi}$, is the scalar dissipation for the mixture fraction fluctuations and appears as such in the balance equation for the mixture fracture variance. The normalized mean reaction rate defined according to (29) becomes at the equilibrium limit

$$\overline{\hat{w}^e} = \left\{\frac{1}{2}\frac{M\overline{\chi}_s}{\bar{U}} + \frac{\hat{\nabla}\bar{F}\cdot\hat{\nabla}\bar{F}}{Pe}\right\}\frac{p_F(F_s;\boldsymbol{x})}{N_D F_s(1-F_s)}, \tag{36}$$

with the reaction rate normalized by the flow timescale, $N_D\overline{\hat{w}}^e$, remaining finite. Here the gradients in $\bar{F}$, $\hat{\nabla}\bar{F}$, are non-dimensionalized by M as in (9). This result is only

dependent on the equal-diffusivity assumption and involves no modelling. The instantaneous scalar dissipation χ is difficult to measure and its joint p.d.f. with the mixture fraction $p_{\chi F}(\chi, F; \boldsymbol{x})$ is needed if $\bar{\chi}_s$ is to be evaluated. Some preliminary measurements of this joint p.d.f. have been made by Yip & Long (1986) in a jet flow. These measurements indicate that the ratio $\bar{\chi}_s/\bar{\chi}$ is near unity in the centre of the jet for all values of F_s but departs from unity by a factor of up to about 2 in the intermittent regions of the flow. Since not even $\bar{\chi}$ is directly measured in the present experiments we can estimate $\widehat{\tilde{w}^e}$ from

$$\widehat{\tilde{w}^e} = \left\{\frac{a}{2}\frac{M\epsilon}{\bar{U}k_t}f'^2 + \frac{\hat{\nabla}\bar{F}\cdot\hat{\nabla}\bar{F}}{Pe}\right\}\frac{p_F(F_s;\boldsymbol{x})}{N_D F_s(1-F_s)}, \tag{37}$$

where

$$a \equiv \frac{\bar{\chi}_s}{\bar{\chi}}\frac{\bar{\chi}k_t}{\epsilon f'^2} \tag{38}$$

and ϵ is the dissipation rate of the turbulence kinetic energy k_t. The second factor in the definition of a is the ratio of the timescale for dissipation of turbulence kinetic energy to that for dissipation of scalar fluctuations. This timescale ratio is dependent on the nature of how the scalar fluctuations are introduced into the flow (Warhaft & Lumley 1978) but has values of the order of 2. Ma & Warhaft (1986) find a value near to 1.6 for the downstream region of scalar mixing layers with a range of initial conditions, but with much lower initial spreading rates than the layer reported here. Accordingly $\widehat{\tilde{w}^e}$ may be estimated from (37) using a value of a equal to the timescale ratio determined for the flow.

The mean scalar dissipation can be determined from the scalar flux measurements. The balance equation for the mean mixture fraction is given by

$$\bar{U}\cdot\nabla\bar{F} + \nabla\cdot(\overline{uf}) - \mathscr{D}\nabla^2\bar{F} = 0 \tag{39}$$

and its variance by

$$\bar{U}\cdot\nabla\overline{f^2} + 2\overline{uf}\cdot\nabla\bar{F} + \nabla(\overline{uf^2}) - \mathscr{D}\nabla^2\overline{f^2} + \bar{\chi} = 0. \tag{40}$$

Multiplying (39) by $(1-2\bar{F})$ and subtracting (40) yields the balance equation for the fluid mixedness:

$$\bar{U}\cdot\nabla\{\bar{F}(1-\bar{F}) - \overline{f^2}\} + \nabla\cdot\{(1-2\bar{F})\overline{uf}\} - \nabla\cdot(\overline{uf^2}) - \mathscr{D}\nabla^2\{\bar{F}(1-\bar{F}) - \overline{f^2}\}$$
$$+ 2\mathscr{D}\nabla\bar{F}\cdot\nabla\bar{F} - \bar{\chi} = 0. \tag{41}$$

In the present experiments all terms other than the scalar dissipation are measured and so $\bar{\chi}$ can be determined from this balance. On the centreline of the layer the second term dominates so that

$$\bar{\chi}_{CL} \approx \left[\frac{\partial}{\partial y}\{(1-2\bar{F})\overline{vf}\}\right]_{CL} \approx -\left[2\overline{vf}\frac{\partial\bar{F}}{\partial y}\right]_{CL}, \tag{42}$$

where v is the velocity fluctuation in the transverse y-direction and use has been made of the symmetry of $\overline{vf}$ about $y = 0$, applicable in an ideal layer.

Probability density functions for the reactant mole fractions Γ_A and Γ_B may be obtained from $p_F(F)$ in the limiting cases for frozen flow by using (12):

$$p_{A^0}(A^0) = p_F(A^0), \quad p_{B^0}(B^0) = p_F(1-B^0), \tag{43a, b}$$

where $$A^0 \equiv \Gamma_A^0/\Gamma_{A_1} = \hat{\Gamma}_A^0, \quad B^0 \equiv \Gamma_B^0/\Gamma_{B_2} = \hat{\Gamma}_B^0. \tag{43c, d}$$

For the equilibrium flow case we obtain, using (13),

$$p_{A^e}(A^e) = (1-F_s)\left\{\delta(A^e)\int_0^{F_s} p_F(F)\,\mathrm{d}F + p_F(F_s+(1-F_s)A^e)\right\}, \tag{44a}$$

$$p_{B^e}(B^e) = F_s\left\{\delta(B^e)\int_{F_s}^1 p_F(F)\,\mathrm{d}F + p_F(F_s-F_sB^e)\right\}, \tag{44b}$$

where $$A^e \equiv \Gamma_A^e/\Gamma_{A_1} = \hat{\Gamma}_A^e, \quad B^e \equiv \Gamma_B^e/\Gamma_{B_2} = \hat{\Gamma}_B^e. \tag{44c, d}$$

In this case the p.d.f.s have Dirac delta functions at zero concentration with strengths corresponding to the total probability of F being less than F_s or greater than F_s for A and B respectively.

Values of the turbulent scalar fluxes $\overline{u\gamma_i}$ can be obtained from the joint p.d.f. of the mixture fraction and the velocity for the limiting cases of frozen and equilibrium flow. Here we shall confine ourselves to consideration of the transverse components of these fluxes. For frozen flow the results are trivially

$$\overline{v\gamma_A^0} = \Gamma_{A_1}\overline{vf}, \quad \overline{v\gamma_B^0} = -\Gamma_{B_2}\overline{vf}. \tag{45a, b}$$

For equilibrium flow we have

$$\overline{v\gamma_A^e} = \overline{v\Gamma_A^e} = (\Gamma_{A_1}+\Gamma_{B_2})\int_{-\infty}^{\infty}\int_{F_s}^1 v(F-F_s)\,p_{vF}(v,F)\,\mathrm{d}F\,\mathrm{d}v, \tag{46a}$$

$$\overline{v\gamma_B^e} = (\Gamma_{A_1}+\Gamma_{B_2})\int_{-\infty}^{\infty}\int_0^{F_s} v(F_s-F)\,p_{vF}(v,F)\,\mathrm{d}F\,\mathrm{d}v. \tag{46b}$$

Results for other turbulent fluxes may be obtained in a similar fashion.

It can be noted from (15) that the mean values of Γ_A and Γ_B must lie between the frozen flow and equilibrium flow values. This is not a necessary condition for the variances, covariances, p.d.f.s and turbulent scalar fluxes. It is, however, a constraint on the mean reaction rate normalized by the chemical timescale, so that

$$\overline{\hat{w}^0} \geqslant \overline{\hat{w}} \geqslant \overline{\hat{w}^e}. \tag{47}$$

When normalization is by the fluid dynamic timescale the inequalities are around the other way.

Since the spatial and temporal resolution of the scalar measurements is limited it is worthwhile to have some other checks on the measurements. Assuming two-dimensionality and transforming (39) to $(x, (y/\delta))$-coordinates where $\delta(x)$ is a measure of the width of the mixing layer (not to be confused here with the Dirac delta function), see figure 1, yields upon multiplying by $(1-2\bar{F})$ and integrating across the layer

$$\int_{-\infty}^{\infty}(-\overline{vf})\frac{\partial\bar{F}}{\partial(y/\delta)}\mathrm{d}(y/\delta) = \tfrac{1}{2}\bar{U}\frac{\mathrm{d}\delta}{\mathrm{d}x}\int_{-\infty}^{\infty}\bar{F}(1-\bar{F})\,\mathrm{d}(y/\delta) + \tfrac{1}{2}\bar{U}\delta\frac{\mathrm{d}}{\mathrm{d}x}\int_{-\infty}^{\infty}\bar{F}(1-\bar{F})\,\mathrm{d}(y/\delta)$$
$$+\frac{\mathscr{D}}{\delta}\int_{-\infty}^{\infty}\frac{\partial\bar{F}}{\partial(y/\delta)}\frac{\partial\bar{F}}{\partial(y/\delta)}\mathrm{d}(y/\delta) \approx \tfrac{1}{2}\bar{U}\frac{\mathrm{d}\delta}{\mathrm{d}x}\int_{-\infty}^{\infty}\bar{F}(1-\bar{F})\,\mathrm{d}(y/\delta). \tag{48}$$

The approximation assumes high Reynolds number and fully developed $\bar{F}$-profiles. Axial variations in the conserved scalar flux have been neglected. Similar balances

for the reactive scalars can be made. Of more direct interest here is the averaged balance equation for the reactants, e.g.

$$\bar{U}\cdot\nabla\bar{\Gamma}_A+\nabla\cdot(\overline{u\gamma}_A)=\bar{w}_A,$$

where the mean fluxes due to molecular diffusion are neglected at high Reynolds number. In the present flow we obtain

$$\bar{w}_A=\bar{U}\frac{\partial\bar{\Gamma}_A}{\partial x}+\frac{\partial}{\partial y}(\overline{v\gamma}_A)+\frac{\partial}{\partial x}(\overline{u\gamma}_A). \tag{49}$$

The term in the streamwise turbulent flux is negligible so that normalizing as in (29) yields

$$\bar{\hat{w}}=-N_{\mathrm{D}}^{-1}(1+\Gamma_{A_1}/\Gamma_{B_2})\left\{\frac{\partial(\overline{v\gamma}_A)/\partial(y/\delta)}{\bar{U}\Gamma_{A_1}(\delta/M)}+\frac{\partial\bar{\hat{\Gamma}}_A}{\partial(x/M)}\right\}. \tag{50}$$

3. Experimental facility and instrumentation

A schematic diagram of the reactive scalar mixing layer experiment is shown in figure 2. The working section is made of thin polyethylene film which is quite passive to ozone and nitric oxide. The film walls are kept taut by the overpressure provided by the fans and the outlet throttle. The doping gases are injected at the fan inlets and are well mixed in the air streams by three right-angle bends following each fan. Swirl and turbulence are reduced by honeycombs and screens at the entry to the wide-angle diffusers, screens at their exit and the two-to-one contraction upstream of the turbulence grid. The two flows are kept separate by a splitter plate until the turbulence grid is reached. The turbulence grid is made from 63×63 mm hollow square-section aluminium on a $M=320$ mm square pitch giving an open area of 65%. The working section is 8 mm long with a diameter of 2.8 m and is equipped with a mechanism enabling accurate two-dimensional traversing of the measurement probes. Flow velocities used varied from $\bar{U}=0.25$–0.55 m s^{-1}, giving a Reynolds number $Re\equiv\bar{U}M/\nu=5300$ to 11700, with ν the kinematic viscosity.

The doping gases used are nitric oxide and ozone which have diffusion coefficients in air at 25 °C, 1 atm of 0.18 and 0.22 cm^2 s^{-1}, respectively. These are sufficiently close so that little differential diffusion will be expected and the results for the conserved scalar theory can be expected to be valid. In the absence of significant ultra violet radiation to drive the back reaction, they undergo the irreversible reaction

$$NO+O_3\rightarrow NO_2+O_2+200\ \mathrm{kJ/mol}$$

with a rate constant k at 20 °C of 0.37 p.p.m.$^{-1}$ s^{-1} (Chameides & Stedman 1977) which increases by 1% for each 1 °C of temperature rise. The concentrations used were in the range 0.5–6 p.p.m. so that the maximum temperature rise for the reaction was less than 0.05 °C. The reactions are thus passive and the mixing characteristics should be independent of the concentrations used and whether reaction was occurring or not. The Damköhler numbers, (10), were in the range 0.3–2.

Measurements of the velocity field are made by using hot-wire anemometers with conventional ×-wire probes for simultaneous measurements of two velocity components. The wires were calibrated over a range of velocities from 0.1 to 0.8 m s^{-1}. This range was obtained using a TSI 1125 calibrator and the pressure drop in the calibration chamber was measured using a MKS Baratron pressure transducer.

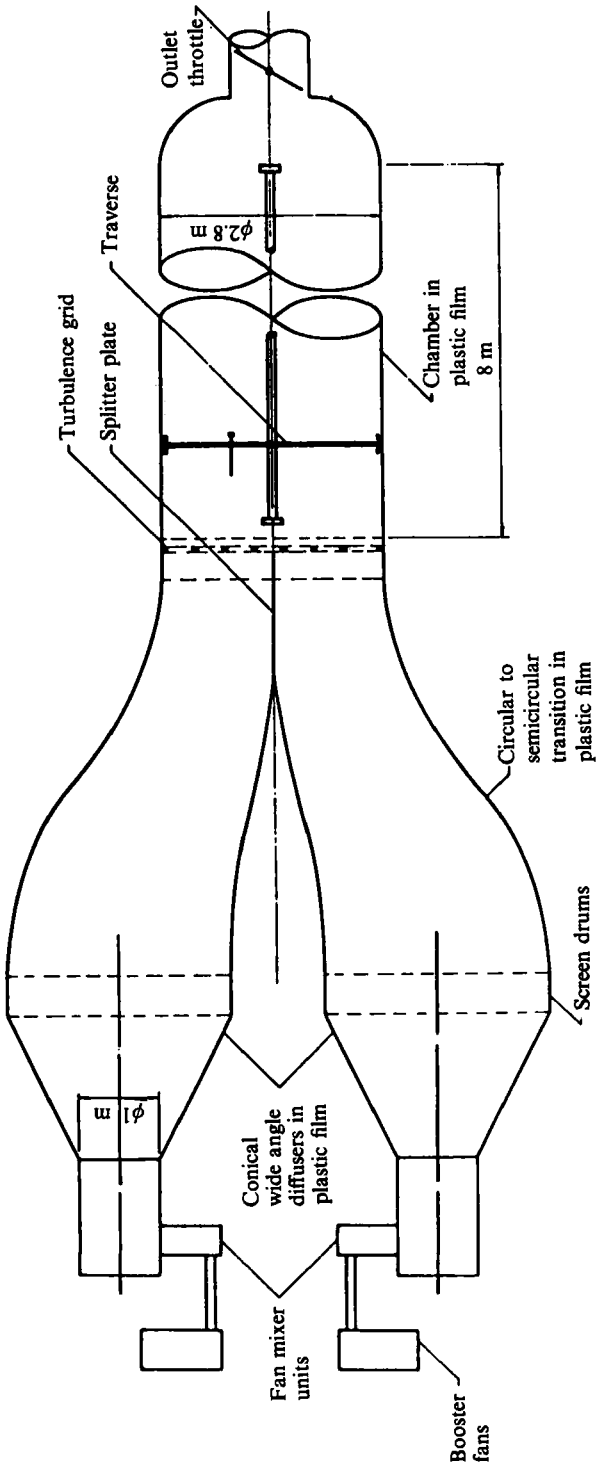

FIGURE 2. Schematic diagram of experimental facility.

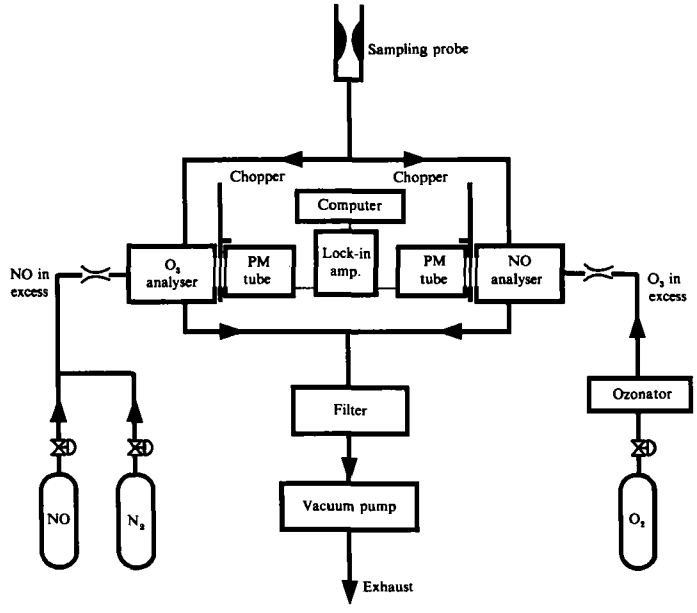

FIGURE 3. Schematic diagram of the chemiluminescent analyser used for concentration measurements.

The mean velocities in the calibration chamber were inferred from the calibration charts plotted as a function of chamber pressure drop. A third-order polynomial fit was used for the hot-wire calibration. The wires were calibrated before and after each experiment and the calibrations found to agree within $\pm 3\%$. The wires were positioned horizontally in the experimental chamber yielding negligible buoyancy effects.

The concentrations of the two reactants were continuously measured using a dual-chamber chemiluminescent analyser constructed using the design criteria of Steffenson & Stedman (1974). The instrument was designed for fast response and is documented in Mudford & Bilger (1983). A simplified diagram is shown in figure 3. Nitric oxide is measured by mixing half of the sample with a high excess of ozone and ozone is measured by mixing with a high excess of NO. The reaction between nitric oxide and ozone yields nitrogen dioxide in an excited state and this decays chemiluminescently. The chemiluminescent decay is in competition with collisional deactivation and so is favoured by low pressures. In these experiments the response of the analyzer has been improved beyond that of Mudford & Bilger (1983) by increasing the pump speed and the flow rates of the reactants in excess, and decreasing the sample flow rate. The reaction cells operated with a pressure of 3.4 kPa, a sample inflow rate for each cell of 80 std $cm^3\ s^{-1}$ and a reactant-in-excess flow rate of 220 std $cm^3\ s^{-1}$ giving a residence time in the cell volume of 62 cm^3 of about 7 ms and a -3 dB response of 23 Hz. This response was confirmed by correlating the response of the sampling system with that of a cold-wire (1.2 μm Pt$-$10% Rh) thermometer of frequency response of about 1 kHz. This response was measured in the mixing layer of one of the fan outlets with electrical heating of the fan inlet air which was also doped with NO and with the fan exhausting into room air. The response corresponds to a sampled volume of the chamber flow of 1.1 cm^3, that is a spatial resolution of 12 mm.

Samples were withdrawn from the flow through 5 m of 6 mm I.D. Teflon tubing with a chocked flow orifice at its inlet end. The flow in the tubing leading to the chemiluminescent analyser was also choked at its outlet end giving rise to a pressure in the tubing which is estimated as 25 kPa. This estimate gives a transit delay time of 220 ms which is close to the delay $\tau_D = 240$ ms measured by comparison of the signals with the cold wire in the tests mentioned above. Some reaction occurs in the sampling tube. The value of $k_s \Gamma_e \tau_D$, where k_s is now $25 \times 0.37/101 = 0.092$ ppm^{-1} s^{-1} and Γ_e is the concentration of the reactant in excess, is always less than 0.1 and the small corrections

$$\delta\Gamma_A = \delta\Gamma_B = k_s \Gamma_A \Gamma_B \tau_D \tag{51}$$

can be added to the data. The effect of this correction is found to be significant for the data obtained here. The mixing that occurs in the sample tube is small and confined to wavenumbers beyond the range of resolution, i.e. to frequencies greater than 23 Hz. This can be concluded from theoretical estimates and from the cross-correlation between the cold-wire and sampled concentration data.

As outlined above, the spatial resolution of the concentration measurements is calculated from the analyser response and sample flow rate to be about 12 mm. Although this is about 6 times the Kolmogorov lengthscale for the flow, spectral calculations indicate that better than 97% of the variance for the conserved scalars should be recovered. Mansour, Bilger & Dibble (1989) find that spatial averaging effects on reactive scalar variances can be estimated quite well by the methods used for non-reactive scalars. For small errors in the variance they also find that there are only minor changes in the shape of probability density functions. Errors in the covariance can be expected to be of the same order as the errors in the variances. Such errors could be significant in determining reaction rates at high Damköhler numbers but give uncertainties of only about 8% for the results obtained here.

The $\times$-wire probe was located 18 mm above the concentration sampling point and the concentration signal corrected for the sampling time lag (~ 240 ms) when making correlations between velocity and concentration. A series of tests showed that at 18 mm or greater separation there was no significant effect of the sample probe flow field on the measured velocity. The separation distance is nearly a factor of 20 down on the integral lengthscales of the turbulence (order $M = 320$ mm), and from measurements made at several separation distances and extrapolation to zero the correlations of velocity and concentration are expected to be within 10% of their true value.

The four signals (two for velocity, two for concentration) were sampled at 128 Hz per channel, digitized by a LSI 11/28 terminal and sent to a VAX 780 computer for further processing of the data. The sampling time at each measuring point was 240 s.

4. Results

4.1. *The flow field*

Details of the flow field are given by Saetran *et al.* (1989). Transverse variations in the mean velocity, $\bar{U}$, are less than 2% outside of the wall boundary layers. Transverse variations in turbulence intensities, $u'/\bar{U}$, $v'/\bar{U}$, $w'/\bar{U}$, are less than 1%. The experiments were confined to the region $12 \leqslant x/M \leqslant 21$ which is well inside the initial period ($x/M < 100$) recognized for the establishment of a classical grid flow and the normal stresses were found to be quite anisotropic with u'/v' varying from 1.85 at

Symbol	Γ_{A_1} (p.p.m.)	Γ_{B_2} (p.p.m.)	N_D	F_s	Re_M	x/M	δ (m)	Comments	Shift in y for $\bar{F} = 0.5$ (mm)
○	3.90	3.85	1.81	0.49	11700	16	1.4	Reactive, $A = NO, B = O_3$	0
⊗	4.08	3.85	1.81	0.49	11700	21	1.4	Reactive, $A = NO, B = O_3$	0
□	0.68	0.70	0.30	0.51	11700	16	1.6	Reactive, $A = NO, B = O_3$	−7
⊠	0.68	0.70	0.30	0.51	11700	21	1.65	Reactive, $A = NO, B = O_3$	−14
△	0.76	1.70	0.53	0.69	11700	21	1.56	Reactive, $A = NO, B = O_3$	−6
+	0.73	0.67	0.32	0.48	11700	16	1.4	Reactive, $A = O_3, B = NO$	−5
▽	1.20	3.00	1.98	0.71	5300	21	1.30	Reactive, $A = NO, B = O_3$	−2
◇	4.3	—	—	—	5300	21	1.23	Non-reactive, $A = NO$	0

TABLE 1. Experimental conditions

$x/M = 12$ to 1.67 at $x/M = 21$ for $Re = 11700$. The turbulence kinetic energy, k_t, varied from 2.37×10^{-3} to 1.43×10^{-3} m^2 s^{-2} while its dissipation estimated from $\epsilon = -\bar{U}\,\mathrm{d}k/\mathrm{d}x$ varied from 4.8×10^{-4} to 2.1×10^{-4} m^2 s^{-3} for $x/M = 12$ to 21 for $Re = 11700$. These dissipation estimates agree quite well with those measured using the isotropic turbulence formula (Hinze 1975)

$$\epsilon = 15\nu\overline{(\partial u/\partial x)^2}$$

and Taylor's hypothesis.

The above values for k_t and ϵ yield integral scales $L_\epsilon \equiv k_t^{\frac{3}{2}}/\epsilon$ of 240–260 mm and Kolmogorov scales $\eta \equiv (\nu^3/\epsilon)^{\frac{1}{4}}$ of 1.6–2.0 mm. The corresponding turbulence Reynolds number $Re_t \equiv u' L_\epsilon/\nu$ varies from 970 to 700. An estimate for the Taylor microscale

$$\lambda \equiv [\overline{u^2}/\overline{(\partial u/\partial x)^2}]^{\frac{1}{2}} \tag{52}$$

using Taylor's hypothesis yielded $\lambda = 25$ mm at $x/M = 21$.

4.2. *Conserved scalars*

Variations in the statistics of the mixture fraction, determined from (8), over a range of inlet concentrations, Γ_{A_1} and Γ_{B_2}, give a sensitive test of the conserved scalar theory (i.e. the equal diffusivity assumption) and the quality of the measurement technique. For a given flow Reynolds number the mixture fraction statistics should be independent of the inlet concentrations and hence N_D, F_s and whether the flow is reactive or not. Table 1 shows the range of experimental conditions tested.

Figure 4 shows the mean mixture fraction profiles at $x/M = 21$ for the conditions of table 1. Data for both $Re = 11700$ and 5300 are included. The centres of the profiles have been shifted such that $y = 0$ for $\bar{F} = 0.5$. Further, the plots have been normalized by the experimentally determined value of δ, the width of mixing layer obtained as the distance between where the profiles go through $\bar{F} = 0.1$ and $\bar{F} = 0.9$. The profiles do not show a large scatter and also appear to be antisymmetric. The profile obtained by LaRue & Libby (1981) in a thermal layer is shown for

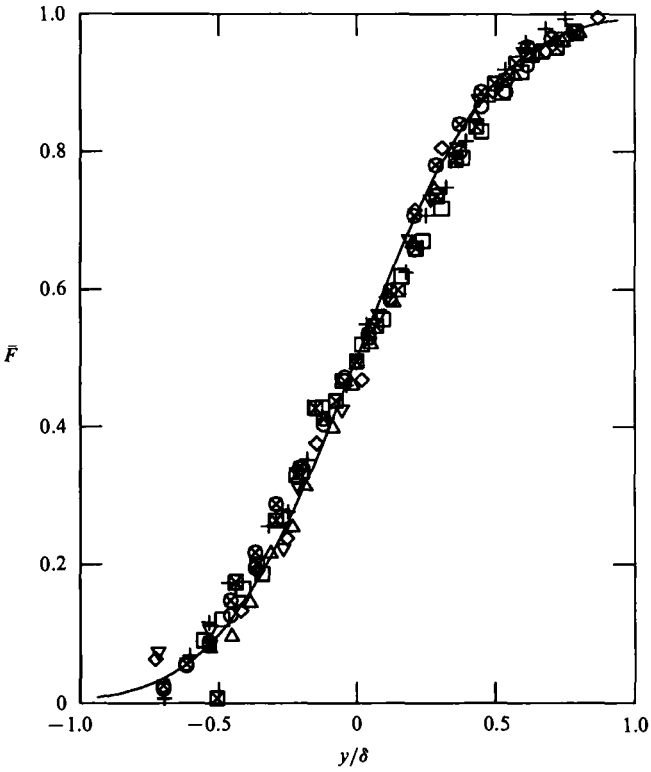

FIGURE 4. Profiles of mean mixture fraction. Symbols as in table 1; ——, LaRue & Libby (1981).

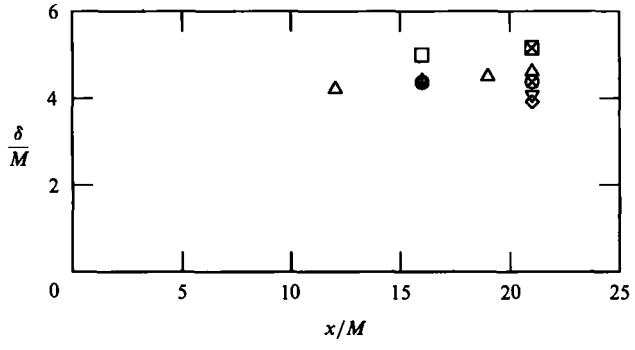

FIGURE 5. Spreading rate (δ/M) of the scalar mixing layer as a function of downstream distance x/M from the turbulence grid. Symbols as in table 1.

comparison. The values of δ and the shift in y are shown in table 1. It is seen that the variations in δ at $Re = 11700$ are about $\pm 8\%$. The shifts in y are small ($< 0.01\delta$) and there is no discernible trend with N_D or $\bar{F}_s$. The variations of this order in δ and y can only be attributed to the accuracy of the measurements. Problems with the measurements include drift in the analyser calibration factor and drift of the unmixed stream concentration, Γ_{A_1} and Γ_{B_2} over the course of a run. Figure 5 shows the variation of δ with x. There is a considerable scatter for δ over the present measurement range but there appears to be no systematic dependence of δ on N_D.

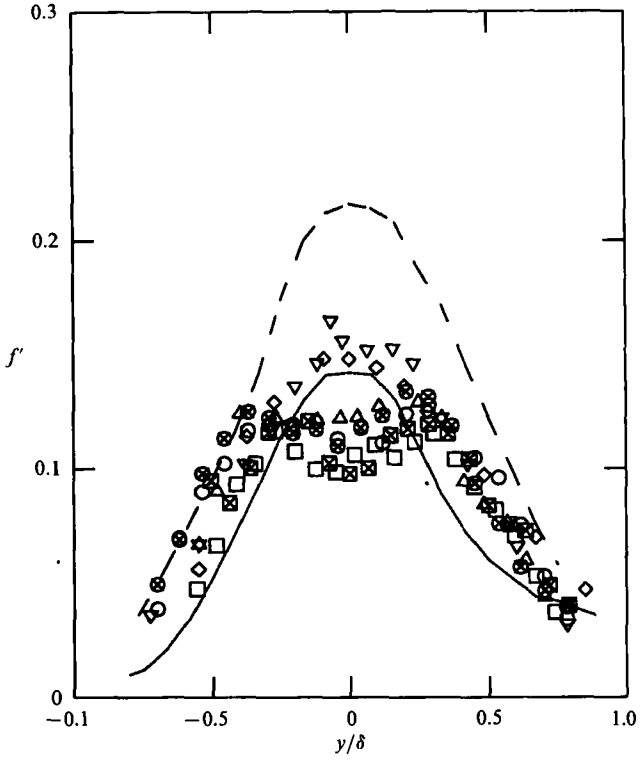

FIGURE 6. R.m.s. fluctuation of mixture fraction at $x/M = 21$. Symbols as in table 1; ----, LaRue & Libby (1981); ——, Keffer *et al.* (1977).

Values of δ/M are higher than found in thermal mixing layers for values of x/M even twice those measured here. This must arise from some aspect of the initial conditions or the overall width of the flow and must be kept in mind when interpreting the present results in the light of the thermal mixing layer results.

Figure 6 showed data for the r.m.s. fluctuation of the mixture fraction, f'. Once again there appears to be no significant effect of N_D and F_s on the profiles. The profiles at the higher Reynolds number show a dip in f' in the centre of the layer while at $Re = 5300$ the profiles peak on the centreline. The profiles appear to be fairly symmetrical, which they should be if the basic flow is homogeneous in the y-direction. Apart from the central dip the profiles are generally similar to those obtained by Keffer *et al.* (1977) at $x/M = 41$ and LaRue & Libby (1981) at $x/M = 30$ except that the latter show asymmetry due to the residual temperature fluctuations in the heated stream. In all these cases the measurements have been made in the initial region $x/M < 100$ and hence one can expect variations in the f' profiles that depend on Reynolds number and the details of the initial conditions. It is noted that in all cases $f' \ll (\bar{F}(1-\bar{F}))^{\frac{1}{2}}$ and the fluid is relatively well mixed.

Figure 7 shows profiles of skewness, $S \equiv \overline{f^3}/f'^3$ and kurtosis, $K \equiv \overline{f^4}/f'^4$ at $x/M = 21$ and 16 for the low and high N_D (0.3 and 1.8) of table 1. Compared with the higher-x/M results of LaRue & Libby (1981) and Ma & Warhaft (1986) there is general similarity except for the kinks in the profiles near $y/\delta = 0$. These kinks are allied to the dip in the r.m.s. profile and must arise from some aspect of the initial conditions or the overall width of the flow. The results indicate no significant effect of N_D or F_s on the mixing field.

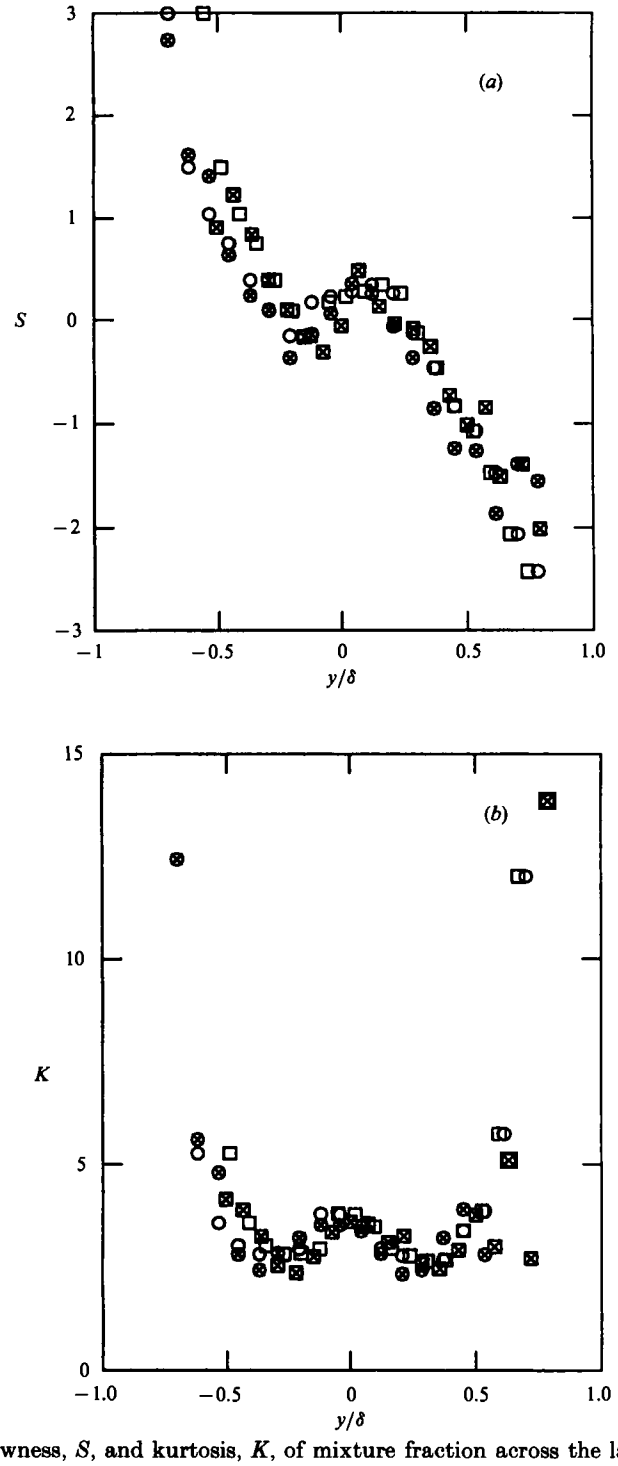

FIGURE 7. Skewness, S, and kurtosis, K, of mixture fraction across the layer at $x/M = 21$ and 16 for $Re = 11700$ runs of table 1.

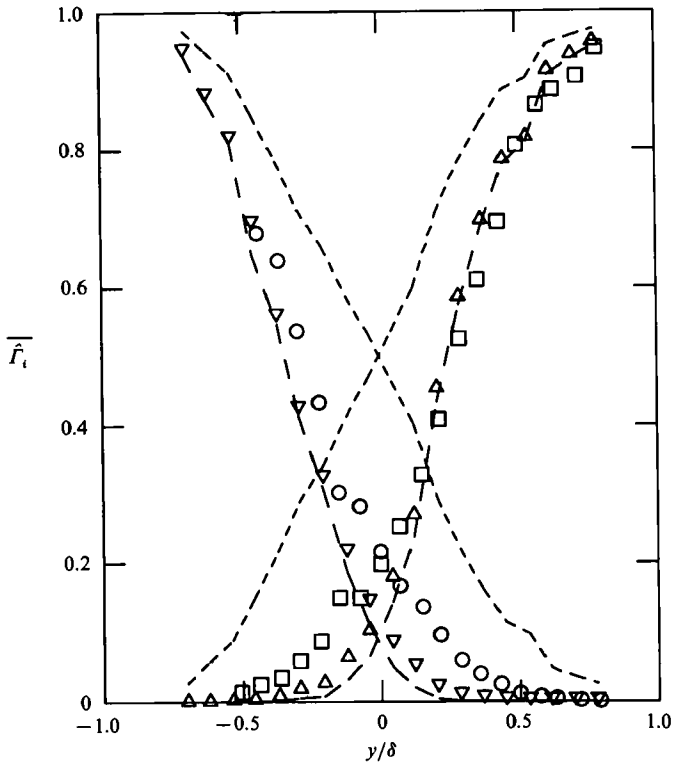

FIGURE 8. Distributions of mean reactant concentrations at $x/M = 21$, $Re = 11700$. $N_D = 1.81$: △, species A; ▽, species B. $N_D = 0.30$: □, species A; ○, species B. The lines show equilibrium (----) and frozen (---) limits as given by equation (18) and (17) respectively.

It can be concluded that, within the limits of experimental error, a conserved scalar determined from reactive scalars shows the same mixing characteristics independent of Damköhler number and of the stoichiometry of the reacting streams, all scalars being passive to the flow. This is as expected from conserved scalar theory on the assumption that small differences in the molecular diffusion coefficients of the species will not have a significant effect in turbulent flow.

4.3. *Reacting scalars*

Figure 8 shows the effect of Damköhler number on the mean species concentrations at $x/M = 21$ for $Re = 11700$. The equilibrium flow and frozen flow limits given by (18) and (17) are shown as determined from the mixture-fraction p.d.f.s obtained at the higher Damköhler number. It is seen that the results for finite Damköhler number obey the constraint obtained from averaging (15) that the mean concentrations lie between the frozen and equilibrium values. Saetran *et al.* (1989) show these results plotted against mean mixture fraction but give the equilibrium limit incorrectly; they neglect to include the contribution due to mixture fraction fluctuations as given by (18). Figure 8 shows that the $N_D = 1.81$ results are quite close to the equilibrium limit at $x/M = 21$. The results for $x/M = 16$ (not shown here) are also found to be close to the equilibrium limit, but not as close as for the results at $x/M = 21$.

Figure 9 shows the r.m.s. fluctuations in the reactant concentrations compared

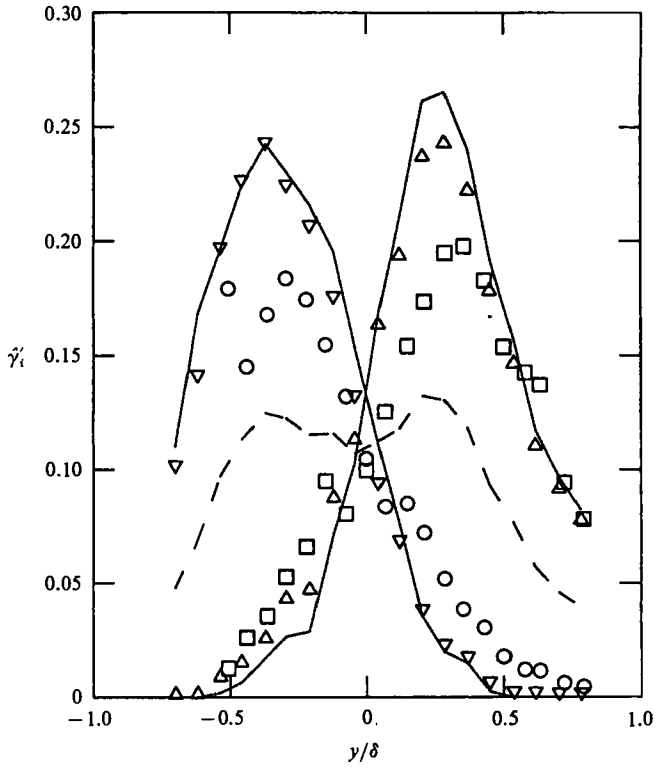

FIGURE 9. Distributions of scalar fluctuation intensities at $x/M = 21$, $Re = 11700$. Symbols as in figure 8. The full lines show the equilibrium flow values and the broken lines, the frozen flow values obtained from (26) and (21) respectively.

with the values for equilibrium and frozen flow, (25) and (21). Although there is no realizability constraint that the finite-Damköhler-number results fall between these limiting cases there appears to be a tendency for them to do so. Once again the high-Damköhler-number results are quite close to the equilibrium limit. The $N_D = 0.30$ case shows considerable effects of finite rate chemistry at $x/M = 21$ and even more at $x/M = 12$.

Figure 10 shows profiles of the normalized reactant covariance for $Re = 11700$ at $x/M = 16$ and 21 for $N_D = 0.30$ and 1.81. It is seen that the data lie between the equilibrium and frozen limits, (26) and (22), having a trend with N_D and x/M which is consistent with there being a monotonic trend with overall reactedness. Values of the correlation coefficient, $R_{AB} \equiv \overline{\gamma_A \gamma_B}/\gamma_A' \gamma_B'$, at $x/M = 21$ may be obtained using the data of figure 9. At $N_D = 0.3$ and $N_D = 1.81$ they have values around -0.8 and -0.6 respectively in the middle of the flow and these lie between the frozen flow value of -1.0, (24) and the equilibrium values, (27), which are around -0.5 in the middle of this flow. The segregation coefficient $\alpha \equiv \overline{\gamma_A \gamma_B}/\bar{\Gamma}_A \bar{\Gamma}_B$ can be obtained using the data of figure 8. It is more sensitive to N_D, with values in the centre of the flow being around -0.6 at $N_D = 1.81$ and around -0.2 at $N_D = 0.30$. These values lie between the equilibrium limit, (26*b*), of -1 and the frozen limit, (23), which is here around -0.05 in the middle of this flow. (It should be noted that figure 7 of Saetran *et al.* (1989) is wrongly labelled for the low-N_D symbols.) Toor (1969) proposed the closure model

$$\overline{\gamma_A \gamma_B} \approx \overline{\gamma_A^e \gamma_B^e} = -\overline{\Gamma_A^e \Gamma_B^e}, \tag{53}$$

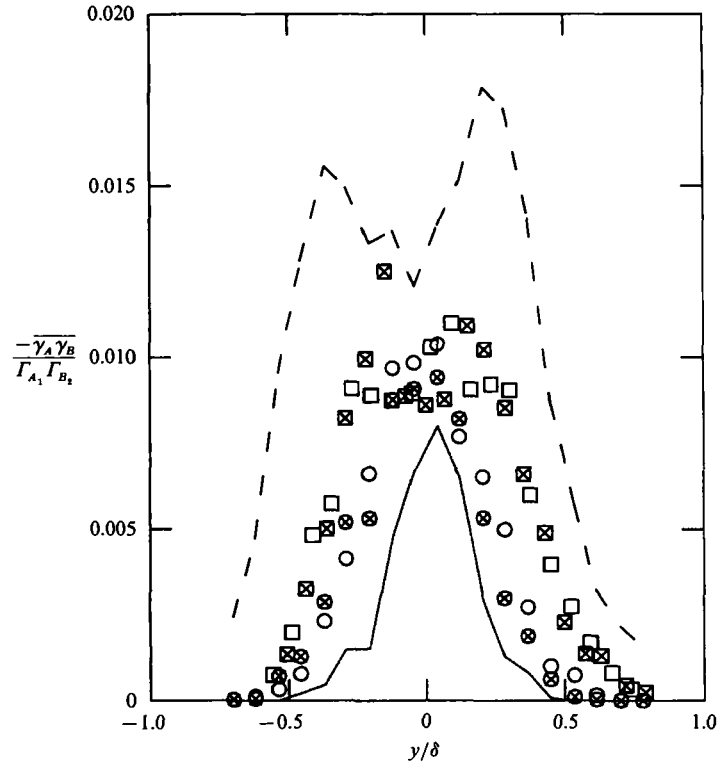

FIGURE 10. Distributions of reactant concentration covariance normalized with inlet concentrations for both $N_D = 0.30$ and $= 1.81$ and for $x/M = 16$ and 21. Symbols as in table 1. The full curve gives the equilibrium flow values and the dashed curved the frozen flow value, both for $x/M = 21$.

and the closure model of Mudford & Bilger (1985) can be shown to be equivalent to this. It appears that a closure model which uses an interpolation between the frozen and equilibrium correlation limits of $\overline{\gamma_A \gamma_B}$ may be an improvement.

Figure 11(*a*) shows the spectra for the reactant concentration fluctuations for $N_D = 0.3$, $y/\delta = 0$. The power spectral density, $E_\gamma(\phi)$, with ϕ the frequency, has been obtained by normalizing by the signal variance. The spectra for both reactants are identical down to the cutoff frequency, 60 Hz. They have only a small range in which the slope is of the order $-\frac{5}{3}$ with the upper cutoff being at about 5 Hz, much below the Kolmogorov frequency of 280 Hz. The corresponding spectrum for the mixture-fraction fluctuation has a $-\frac{5}{3}$ power-law region extending to 20 Hz, close to the instrument resolution of 23 Hz. The cross-spectral density function between γ_A and γ_B has been decomposed into the coherence function and phase (Bendat & Piersol 1971) and are shown in figure 11(*b*, *c*). These show a sudden change from high coherence, 180° out of phase at $\phi < 10$ Hz, to incoherent random phase for $\phi >$ 10 Hz. The correlation coefficient R_{AB} is -0.82 here and it can be seen that it arises almost entirely from $\phi < 10$ Hz. The break at 10 Hz cannot be attributed to instrument response or noise. It is likely to be associated with a reactive–diffusive balance between spectral transfer from large, low-frequency eddies and chemical reaction. Corrsin (1961, 1964) considers this balance for a first-order chemical reaction. Reformulation for second-order reactions does not appear to be straightforward and that outlined in Bilger (1980, p. 104) is not supported by these data. At

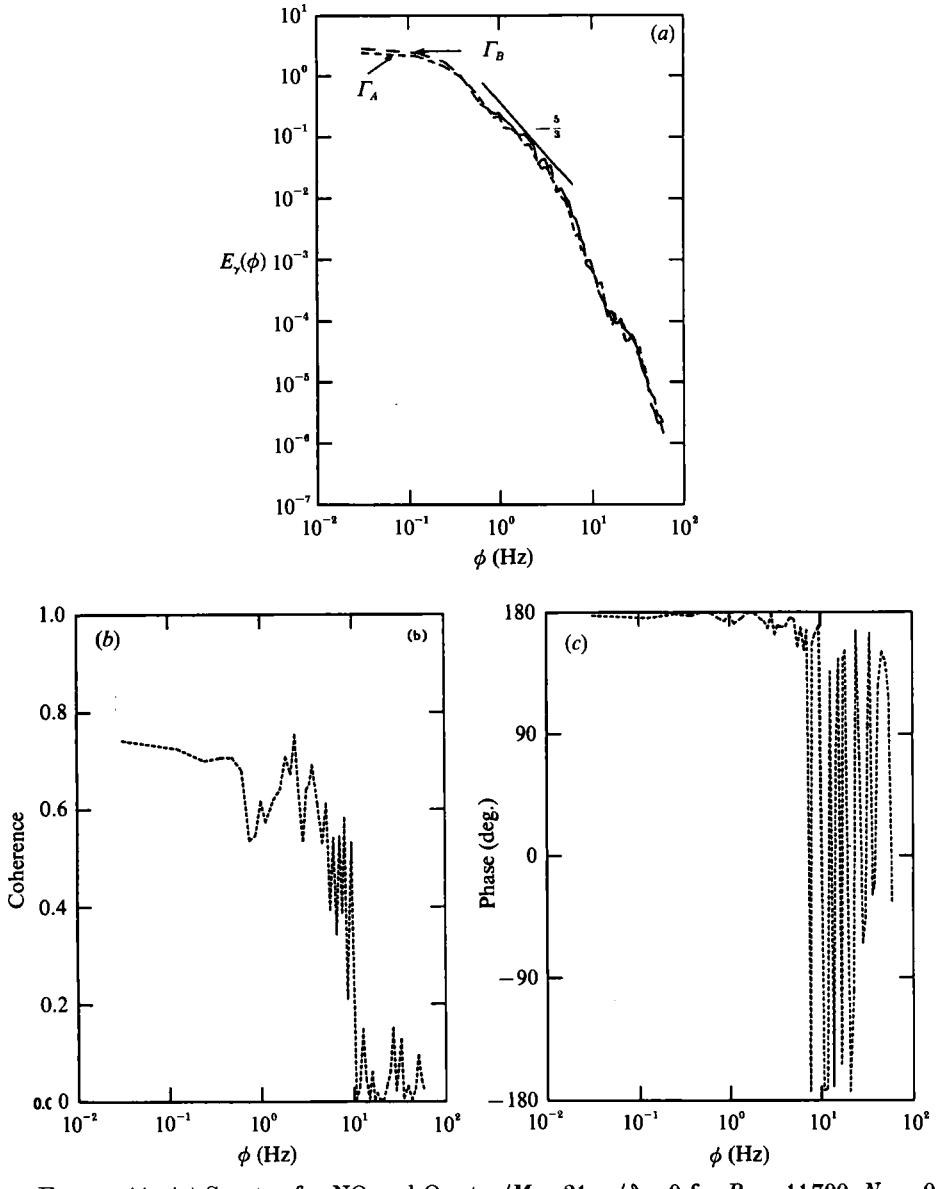

FIGURE 11. (*a*) Spectra for NO and O_3 at $x/M = 21$, $y/\delta = 0$ for $Re = 11700$, $N_D = 0.3$, with (*b*) associated coherence and (*c*) phase.

$N_D = 1.81$ the cross-spectra are similar with the break in coherence occurring at about the same frequency but being less sudden.

Figure 12 shows probability density functions for the reactants for high and low Damköhler number at various positions across the layer at $x/M = 21$ for $Re = 11700$. Also shown are the p.d.f.s for the mixture fraction deduced from the same data. Equilibrium and frozen flow p.d.f.s can be deduced from the mixture-fraction p.d.f using the transformations of (43) and (44) and p.d.f.s for these are also shown. The arrows on the ordinate at $x = 0$ denote the Dirac delta functions. It is seen in figure 12(*a*, *b*) that on the centreline of the flow the p.d.f.s are close to the equilibrium p.d.f.s at the high Damköhler number, allowance being made for the smearing of the

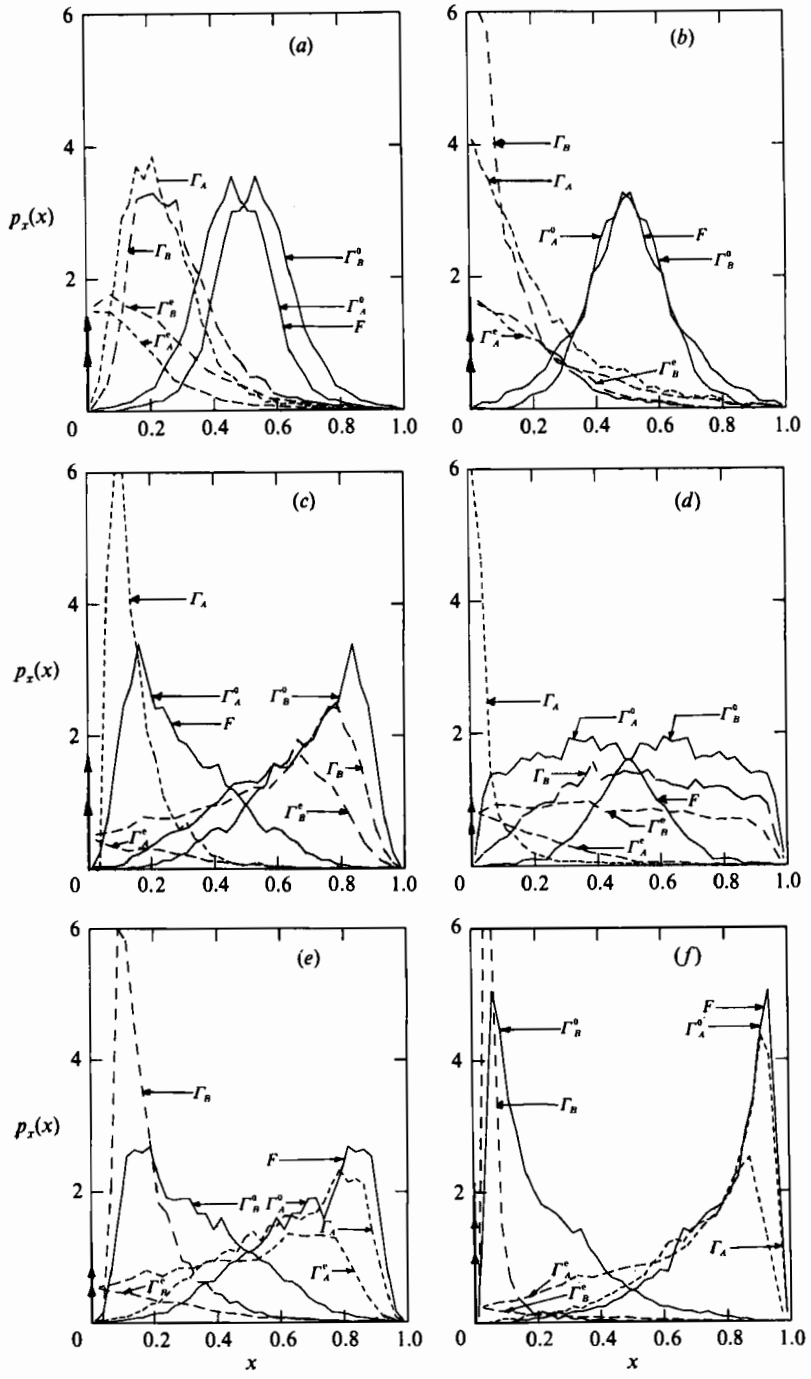

FIGURE 12. Probability density function of mixture fraction (——) and reactants A (– – – –) and B (— — —) at $x/M = 21$. (*a*) $y/\delta = 0$, $N_D = 0.3$; (*b*) $y/\delta = -0.04$, $N_D = 1.81$; (*c*) $y/\delta = -0.36$, $N_D = 0.3$; (*d*) $y/\delta = -0.37$, $N_D = 1.81$; (*e*) $y/\delta = 0.43$, $N_D = 0.3$; (*f*) $y/\delta = 0.45$, $N_D = 1.81$. Also shown are frozen and equilibrium flow p.d.f.s derived from (43) and (44).

delta functions by noise. At the low Damköhler number the shape of the p.d.f. is like that for the frozen flow limit but shifted downward about 0.3 in $\hat{\Gamma}_i$. Away from the centreline the p.d.f.s for the deficient reactant are seen in figure 12(*c–f*) to be near to those for equilibrium flow at both the high and low Damköhler number, allowing once again for smearing of the delta function by noise. For these cases the mixture fraction is typically 0.8 or 0.2 so that the deficient reactant has a time constant of $(0.6k\Gamma_{A_1})^{-1}$ or $(0.6k\Gamma_{B_2})^{-1}$, the excess of the other reactant being 0.6 of its free-stream value. At the low Damköhler number this time constant is about 7 s and the convection time from the grid is only 12.2 s at $x/M = 21$. Thus it is seen that the fluid in the outer parts of the scalar layer can almost never have resulted from a recent mixing event between unmixed stream 1 and stream 2 fluids. The high reactedness in this part of the layer suggests that mixing there occurs between parcels of already mixed fluid or of mixed fluid and unmixed fluid from the neighbouring free stream. This is consistent with the width of the layer being much larger than the integral scale of the turbulence. As noted already $\delta/M \sim 4$ and $L_\epsilon/M \sim 0.8$ so that $\delta \sim 5L_\epsilon$ and mixing between neighbouring fluid parcels would be expected.

Joint p.d.f.s of the reactants are shown in figure 13 for $y/\delta = 0$, $x/M = 21$, $Re = 11700$ and low and high Damköhler numbers. At the edges of the layer the joint p.d.f.s are essentially given by the single variate p.d.f.s of figure 12(*c–f*) since they show no variation from zero in the deficient reactant. Joint p.d.f.s plotted in the form of figure 13 are confined to the half of the square near the region. At the frozen flow limit the p.d.f. is constrained to lie on the diagonal $\hat{\Gamma}_B = 1-\hat{\Gamma}_A$. At the equilibrium flow limit it is confined to lying on the unit intervals along the axes. It is seen that even at the low Damköhler number the p.d.f. lies nearer the equilibrium flow limit. For $N_D = 1.81$ it is very near this limit. From (8) we have

$$\hat{\Gamma}_B = \frac{1-F_s}{F_s}\hat{\Gamma}_A + 1 - \frac{F}{F_s} \tag{54}$$

so that lines of constant mixture fraction have slope $(1-F_s)/F_s$ on these diagrams, or 0.98 for the low-Damköhler-number case. Such a line through the origin corresponds to stoichiometric mixtures. It is seen that stoichiometric mixtures are the least fully reacted.

On figure 13(*a*) we have plotted the compositions $\hat{\Gamma}_A^m, \hat{\Gamma}_A^m$ corresponding to instantaneous mixing to the local mixture fraction and then reaction for the time corresponding to convection from the grid at the mean velocity $\bar{U}$. These concentrations are given by the following formulae:

For $F < F_s$ or $F > F_s$:

$$\hat{\Gamma}_A^m = \frac{F(F_s-F)}{F_s(1-F)\exp\{(F_s-F)N_D x/M\} - F(1-F_s)}, \tag{55a}$$

$$\hat{\Gamma}_B^m = (F_s-F)/F_s + (1-F_s)\hat{\Gamma}_A^m/F_s. \tag{55b}$$

For $F = F_s$:

$$\hat{\Gamma}_A^m = \frac{F_s}{1+F_s(1-F_s)N_D x/M}, \tag{55c}$$

$$\hat{\Gamma}_B^m = \frac{1-F_s}{1+F_s(1-F_s)N_D x/M}. \tag{55d}$$

One might expect the resulting $\hat{\Gamma}_B^m$ versus $\hat{\Gamma}_A^m$ relationship to give the maximum reactedness for the fluid. Figure 13(*a*) indicates that it is more like the median

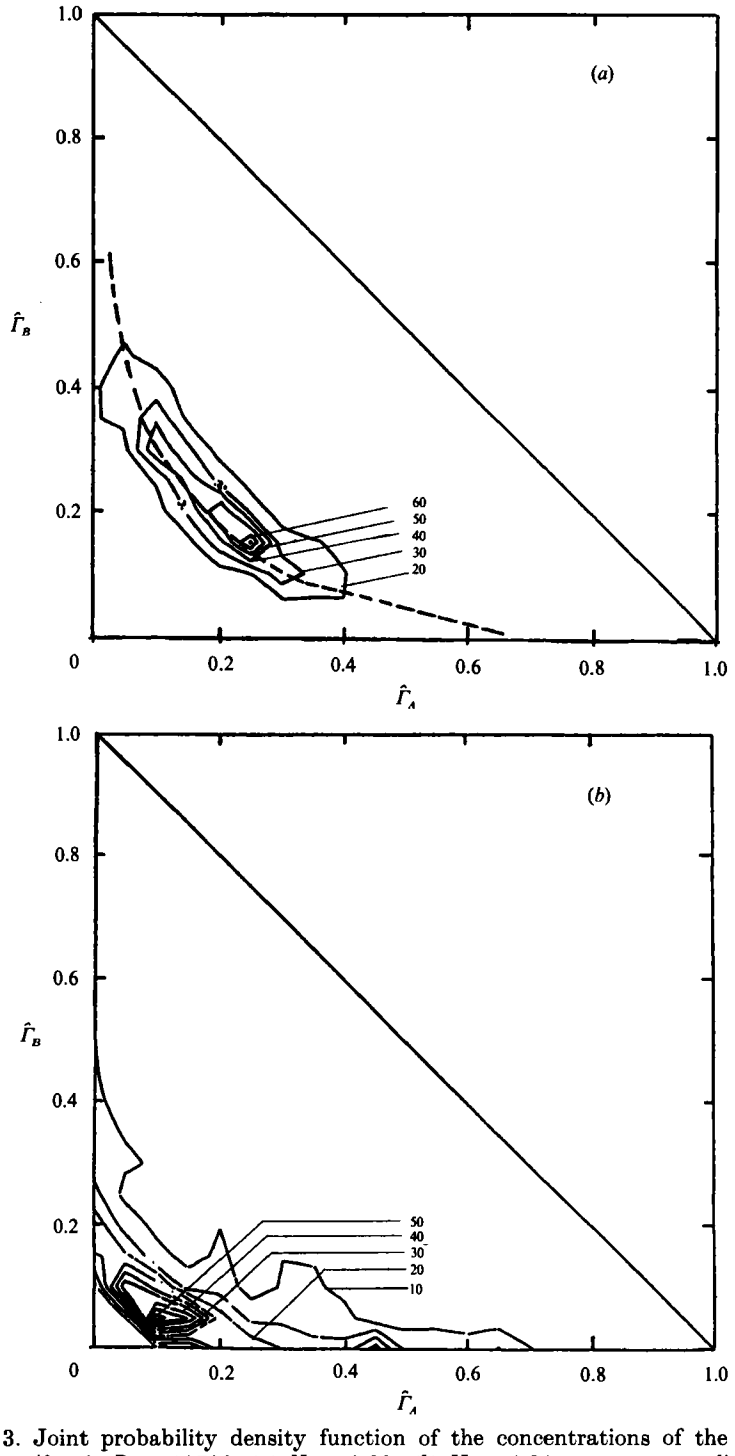

FIGURE 13. Joint probability density function of the concentrations of the two reactants at $x/M = 21$, $y/\delta \approx 0$, $Re = 11700$. (*a*) $N_D = 0.30$; (*b*) $N_D = 1.81$; ----, normalized instantaneous mixing contour derived from (55).

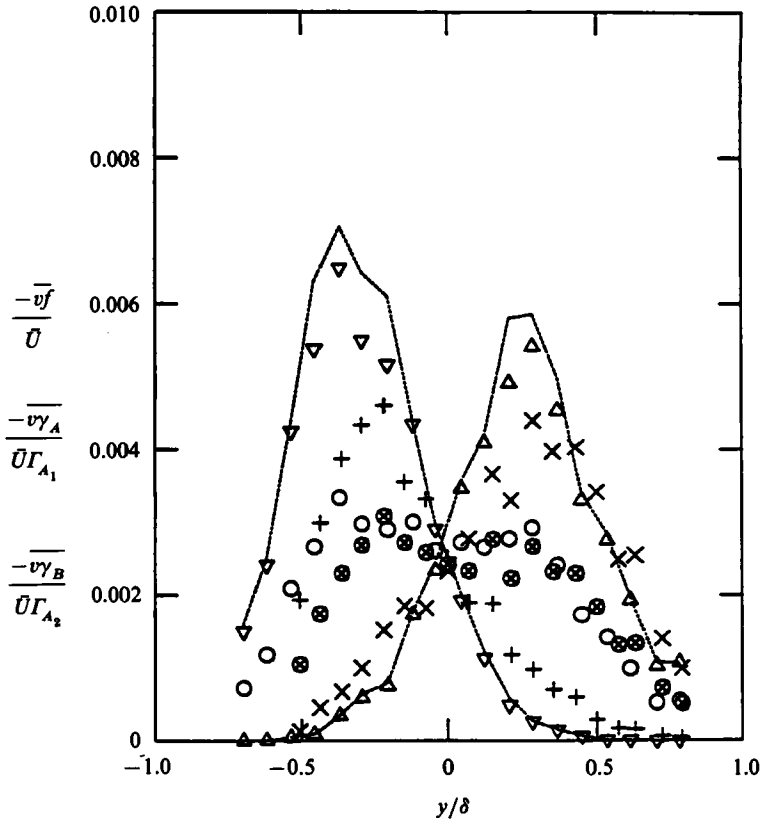

FIGURE 14. Profiles of cross-stream turbulent fluxes at $x/M = 21$ for $Re = 11700$. $N_D = 1.81$: △, species A; ▽, species B; ○, mixture fraction. $N_D = 0.3$: ×, species A; +, species B; ⊗, mixture fraction.

reactedness. For the high Damköhler number the $\hat{\Gamma}_B^m$ versus $\hat{\Gamma}_A^m$ curve is not shown as it lies very close to the axes with coordinates $\hat{\Gamma}_A^m = 0.047$, $\hat{\Gamma}_B^m = 0.049$ for stoichiometric mixtures. Once again the Γ_A^m *vs.* Γ_B^m curve is not a complete envelope for the fluid. It is evident from figure 5 that the layer spreads rapidly at first and more slowly later so that most of the entrainment occurs at low x/M. The instantaneous mixing model may not be the most efficient for reacting the fluid. Furthermore, convective times will show a statistical distribution around the mean value $x/\bar{U}$. On these grounds we may accept the data as credible. This result indicates, however, that for this experiment mean reaction rates are balanced mostly by advection with a timescale for mean flow from the grid, $x/\bar{U}$, rather than mixing with a molecular mixing timescale $\bar{\chi}^{-1}$ or k_t/ϵ. This latter timescale may be more important in shear flows where local entrainment is much stronger.

4.4. *Turbulent fluxes*

Figure 14 shows profiles of turbulent fluxes for the reactants and the mixture fraction obtained from correlations of the hot-wire v-component measurements and the concentration measurements. The equilibrium flow values of the reactant fluxes are those deduced from (46). The mixture fraction fluxes are also those for the reactants under frozen flow conditions, see (45). It is found that the high-Damköhler-number results are very close to those for equilibrium flow (not shown) while those for the low Damköhler number are nearer to the frozen flow case. This is consistent with the

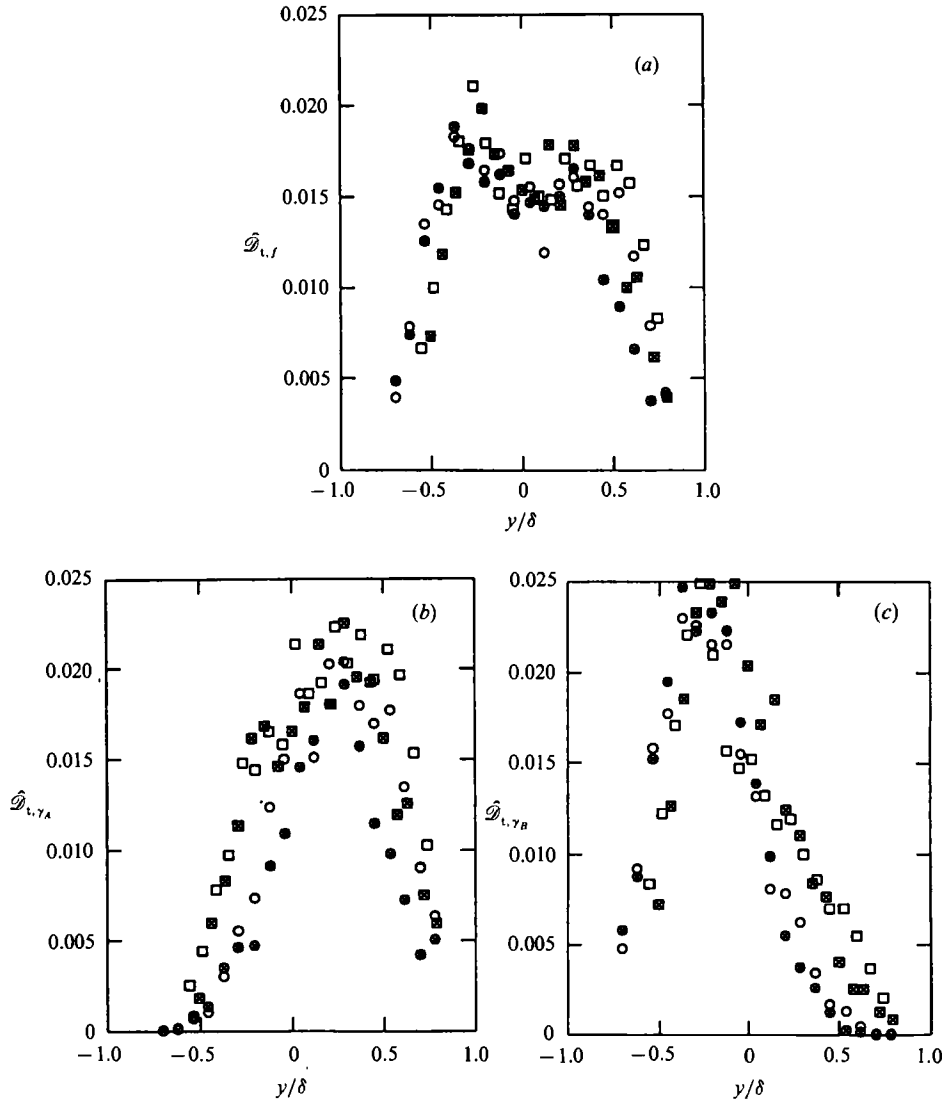

FIGURE 15. Profiles of normalized turbulent diffusivity at $x/M = 16$ and 21 with $N_D = 1.81$ and 0.3 for $Re = 11700$. Symbols as in table 1. (*a*) Diffusivity deduced from (56); (*b*, *c*) deduced for the reactants.

earlier observation that the deficient species concentrations are always close to zero away from the middle of the layer. Use of (48) and the measured mixture-fraction flux yields $d\delta/dx = 0.026$ and this is about half the value that is indicated in figure 5, although there is a large scatter in the data.

Since the scalar mixing layer width is larger than the integral scale of the turbulence it can be expected (Corrsin 1974) that the turbulent flux of the conserved scalar will fit the gradient model quite well. Figure 15(*a*) shows the normalized turbulent diffusivity deduced from

$$\hat{\mathscr{D}}_{t,f} \equiv -\overline{vf}/\{\bar{U}M\,\partial\bar{F}/\partial y\}. \tag{56}$$

It is seen to be fairly uniform in the centre of the layer, indicating that gradient modelling works well there. It also appears to be independent of the Damköhler

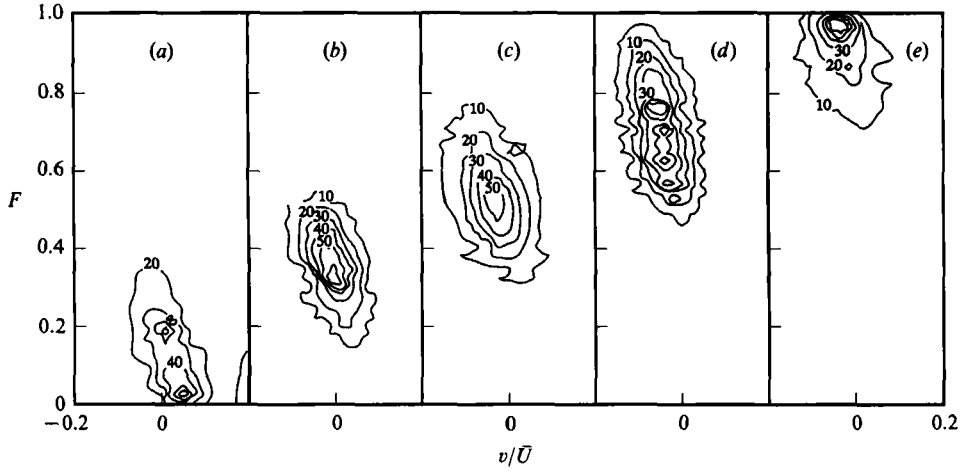

FIGURE 16. Joint probability density functions of cross-stream velocity component and mixture fraction at $x/M = 21$ for $Re = 11700$. (*a*) $y/\delta = -0.46$, (*b*) -0.21, (*c*) 0.04, (*d*) 0.21, (*e*) 0.5. Data from measurements with $N_D = 1.81$.

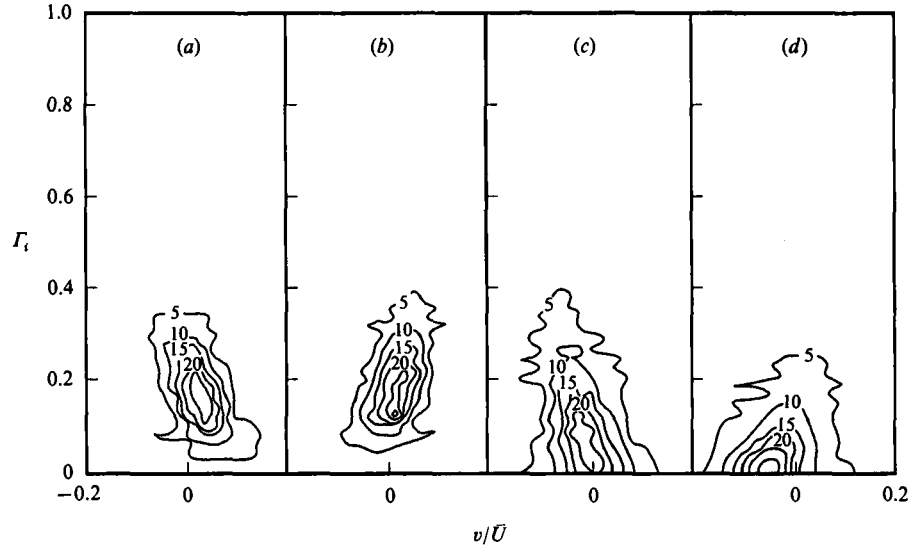

FIGURE 17. Joint probability density function of cross-stream velocity and reactive scalar concentrations at $y/\delta \approx 0$. (*a*, *b*) $N_D = 0.3$; (*c*, *d*) $N_D = 1.81$; (*a*, *c*) species A; (*b*, *d*) species B.

number, which is as expected from conserved scalar theory. Using the values of k_t and ϵ reported in §4.1 in the usual model for the eddy viscosity (Jones & Launder 1972)

$$\nu_t = 0.09k_t^2/\epsilon,$$

the turbulent Schmidt number $\sigma_{tf} \equiv \nu_t/\mathscr{D}_{t,f}$ is found to be about 0.35. This is slightly lower than the value of about 0.5 used for planar flows (Launder 1976).

Figure 15(*b*, *c*) shows the turbulent diffusivities deduced for the reactants. It is seen that they are substantially higher than those for the mixture fraction on the side of the layer from which the reactant comes but are much lower on the other side. In this latter region the diffusivities also show a dependence on N_D, with values for high N_D being smaller than those for low N_D. No evidence of counter-gradient diffusion is found, however.

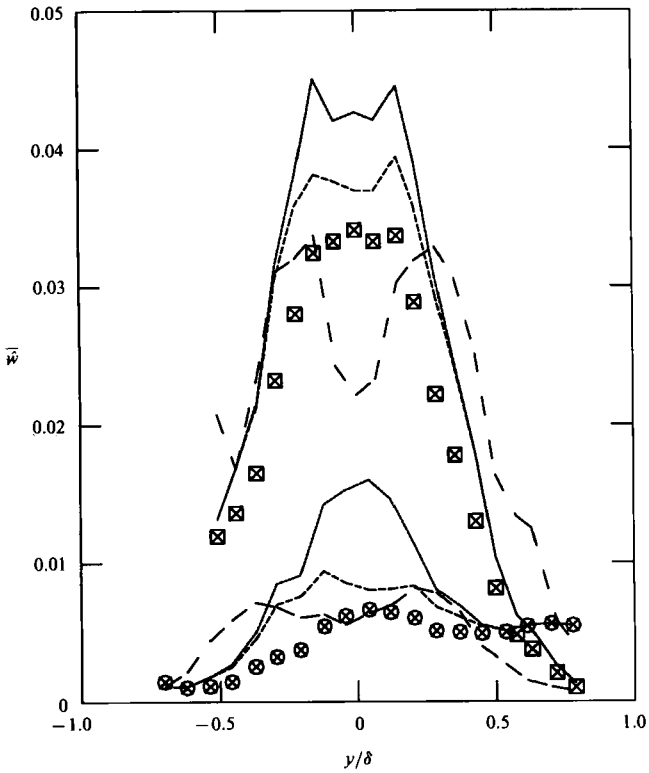

FIGURE 18. Normalized mean reaction rate profiles at $x/M = 21$ and $Re = 11700$; □, $N_D = 0.3$; ⊗, $N_D = 1.81$; ———, equilibrium flow limit (37); ——, product means closure; – – – –, Toor closure.

Figure 16 shows the joint probability density function for mixture fraction and cross-stream velocity component at several positions across the layer. In the centre of the layer the distribution is close to jointly Gaussian with a negative correlation coefficient. The line

$$f = F - \bar{F} = \frac{\bar{U}f'}{v'} R_{vf}\left(\frac{v}{\bar{U}}\right)$$

on such a joint p.d.f. is the equation of conditional means and closely follows the ridge line of the contours. In the centre of the layer the correlation coefficient is -0.52 and $(f'\bar{U}/v')R_{vf} = -0.99$. As we approach the A-stream side of the layer the p.d.f. of v as a whole remains Gaussian and p.d.f.s of v conditional on a given value of F also appear to remain Gaussian. The p.d.f. of F as a whole becomes highly skewed and eventually has a large intermittency spike associated with pure stream-A fluid. The ridge line of the contours remains with a negative slope $(f'\bar{U}/v')R_{vf}$ being -0.6 at $y/\delta = 0.45$ where $R_{vf} = -0.28$.

Figure 17 shows the joint p.d.f. of cross-stream velocity and reactant species concentration on the centreline for low and high Damköhler numbers. In the limit of fast chemistry, that is equilibrium flow, the joint p.d.f. for species A and v would be obtainable by applying the transformation of (13a) to figure 16. The part of the joint p.d.f. of F and v which has F less than F_s is collapsed to the $\Gamma_A = 0$ axis while that part which has F greater than F_s is stretched out and maps into the $\Gamma_A > 0$ domain. There is a similar result for species B except that now it is the part of the joint p.d.f. with $F \geqslant F_s$ which collapses on to the $\Gamma_B = 0$ axis and the part with $F <$

F_s is flipped up (by reflection about $F = F_s$) and stretched out into the $\Gamma_A > 0$ domain. Figure 17 (*c*, *d*) very closely resembles this in relationship to figure 16 (*a*): species A and B are close to fast chemistry at $N_D = 1.81$ as already noted. It is thus seen that in the equilibrium flow limit the reactant-species correlations with v are determined largely by the mixture-fraction correlations. If the mixture fraction has a negative correlation and hence down-gradient flux and the ridge line on its joint p.d.f. plot is more or less straight then it will yield down-gradient fluxes for the reactants at the fast chemistry limit. A counter-gradient flux, of course, would be found for the reactants if the mixture fraction itself was counter gradient. For a down-the-gradient flux in mixture fraction, counter-gradient fluxes for the reactants could be found when the ridge line of the joint F, v p.d.f. is curved. If it is crescent shaped one reactant species would have its down-gradient flux enhanced and the other could become counter gradient. If it is S shaped then both reactants could become counter gradient in their fluxes. Inspection of figure 16 (*b–d*) indicates that there is some tendency of the joint p.d.f. of F and v to become S shaped in its ridge line. This may explain the decreased turbulent diffusivity for the deficient species.

For finite Damköhler numbers the mapping from the joint p.d.f. of F and v to that of $\hat{\Gamma}_i$ and v is not direct. The joint p.d.f. of $\hat{\Gamma}_i$ and F lies in the domain allowed by (12), (13) and (15). From figure 13 it can be seen that the joint p.d.f. of $\hat{\Gamma}_i$ and F will be confined to a narrow region around a basic $\hat{\Gamma}_i$ versus F relationship. It would need a strong correlation between departures from this relationship and v to change a down-the-gradient v,f correlation into a counter-gradient one. Thus positive values of v are associated in general with low values of F but they would need to be associated with more-reacted-than-average species concentrations at these values of F for the flux to become counter gradient. There is little evidence of this in figure 17 (*a*, *b*). They appear close to being a direct mapping from figure 16 (*a*) with a simple $\hat{\Gamma}_i$ versus F relationship.

4.5. *Mean reaction rates*

Figure 18 shows the values of the mean reaction rate calculated from the measured concentrations and normalized in the manner of (29). They are for $x/M = 21$ and $Re = 11\,700$. The results for $N_D = 1.81$ at high y/δ do not tend to zero as they should. This is due to a problem with drift in the zero calibration for species B (ozone) of about 0.5% of its stream-B concentration which has not been corrected.

Using (50) and the fluxes shown in figure 14 it is found that on the centreline the divergence of the turbulent flux balances only about 15% of the mean reaction rate at $N_D = 0.3$, rising to 30% at $N_D = 1.81$. It appears that mean convection dominates. The data are not precise enough for accurate values of $\partial\hat{\Gamma}_A/\partial(x/M)$ to be obtained but the values required to balance (50), 6×10^{-3} at $N_D = 0.3$ and 4×10^{-3} at $N_D = 1.81$, are within the limits of measurement error.

Also shown in this figure is the fast chemistry limit to the reaction rate calculated from (37) with $a = 1.0$ which is the value of the ratio at the timescale of kinetic energy dissipation to that for scalar dissipation evaluated for the centreline using (42) and the values of ϵ and k_t reported in §4.1. Equation (42) yields $M\bar{\chi}_{CL}/\bar{U} \approx 1 \times 10^{-3}$. This value of timescale ratio is lower than the 1.6 found by Ma & Warhaft (1986) at high x/M for this flow and the generally accepted value used in modelling of about 2; but it is within the range found experimentally for more complex flows. In the present case the momentum differences and scalar differences, giving rise to the velocity and scalar fluctuations, are initially at very different scales unlike boundary layers, jets and grid turbulence with quasi-homogeneous scalar properties. A value of unity for the timescale ratio is thus quite credible.

For the frozen flow case the normalized reaction rate is given by (30) which has a value of 0.24 in the middle of the layer. This limit is not plotted in figure 18 since it is off the scale in most of the range of y/δ. It is seen that near the centreline the measured data comply with the constraint, (47), that the reaction rate lies between the equilibrium and frozen flow limits. If a is taken as 2 in evaluating the equilibrium limit from (37) this constraint would be violated. It is seen that lower values of a are required near the edge of the layer, probably due to the rate of conditional to unconditional expectation of χ.

Also shown in figure 18 are the predictions of two commonly used closure assumptions. The product of means closure neglects the contribution of the covariance $\overline{\gamma_A \gamma_B}$ so that the normalized reaction rate is simply $\hat{\Gamma}_A \hat{\Gamma}_B$. It is seen that this simplistic closure overestimates the reaction rate quite significantly particularly at the high Damköhler number, where it is too high by a factor of 2.5 on the centreline. The closure of Toor (1969) sets the covariance $\overline{\gamma_A \gamma_B}$ equal to its equilibrium value $\overline{\gamma_A^e \gamma_B^e}$ as evaluated in (26) and shown in figure 10. The closure of Mudford & Bilger (1985) can be shown to be equivalent to this. Although the Toor closure gives the correct limit for $\overline{\gamma_A \gamma_B}$ at high N_D, it does not necessarily give the correct limit for $N_D \hat{w}$. Mudford & Bilger (1985) define and evaluate the errors involved in this closure for a flow with an opposed jet configuration. They find no clear trend with N_D. Figure 18 indicates that the Toor closure overestimates the reaction rates, but the accuracy of the results is not sufficient for this to be stated with certainty or any trend with N_D to be asserted.

5. Conclusions

It is concluded that, in spite of the limitations resulting from the experimental compromises (low x/M, low number of meshes across the flow, moderate resolution of the scalar measurements) the results for the conserved scalar are generally similar to those measured more accurately in much more ideal scalar mixing layers. Caution should be exercised, however, in interpreting the conserved and reactive scalar results in terms of such an ideal scalar mixing layer owing to the small but perhaps significant effects of these limitations.

Furthermore, it is concluded that, within the limits of experimental error, conserved scalar theory is valid in this flow. The scalars are passive with respect to the flow, and statistics of the conserved scalar, here reported as a mixture fraction, are independent of the Damköhler number of the flow and of the relative concentrations in the two streams, including cases of no reaction. The effects of small differences in the diffusivities of the species are thus apparently not significant.

It is also found that the equilibrium and frozen flow statistics for the reactive scalars, definable by conserved scalar theory in terms of the statistics of the mixture fraction, tend to be limiting values for the finite Damköhler number statistics of the reactive scalars even when they are not theoretically required to be so. This result for the covariance $\overline{\gamma_A \gamma_B}$ as depicted in figure 10 is particularly interesting and could result in improvements to Toor's closure for the mean reaction rate by interpolation between the frozen equilibrium limits. Evaluation in more complex flows is warranted. It appears that the mixing-controlled limit to the reaction rate deduced from the conserved scalar theory, (36), may give good estimates at high Damköhler number provided that uncertainties in the modelling of scalar dissipation and its conditional expectation can be clarified.

Gradient modelling of the turbulent flux of the conserved scalar works quite well

in this flow with a turbulent Schmidt number of 0.35 and the eddy viscosity determined from measured values of the turbulence kinetic energy and its dissipation. This is as may be expected since the scalar layer is much wider than the integral lengthscale of the velocity field. For the reactive scalars it is found that the effective turbulent Schmidt numbers are much lower than this on the side of the layer in which the species is deficient. On its own side the turbulent Schmidt numbers for the reactive scalars are substantially higher than for the conserved scalar. No counter-gradient fluxes were found, although the reductions in turbulent Schmidt number indicate a tendency in that direction.

The results indicate that the reactant concentrations are not bounded by the concentrations that would be obtained if mixing occurred instantaneously at the turbulence grid to the downstream measured value of the mixture fraction, with subsequent reaction for the time of convection by the mean velocity. It is probable that this is consistent with the early rapid mixing of the layer and the statistical fluctuations in the convection time.

Generally it is concluded that conserved scalar theory is an excellent basis upon which to gain insight into reacting turbulent flows with non-premixed reactants.

This work is supported by grants from the Australian Research Council. The contributions of Dr S. H. Stårner in design and commissioning of the facility are gratefully acknowledged.

REFERENCES

BENDAT, J. S. & PIERSOL, A. G. 1971 *Random Data: Analysis and Measurement Procedures*, p. 32. Wiley Interscience.

BILGER, R. W. 1976*a* Turbulent jet diffusion flames. *Prog. Energy Combust. Sci.* **1**, 87–109.

BILGER, R. W. 1976*b* The structure of diffusion flames. *Combust. Sci. Technol.* **13**, 155–170.

BILGER, R. W. 1980 Turbulent flows with nonpremixed reactants. In *Turbulent Reacting Flows* (ed. P. A. Libby & F. A. Williams), pp. 65–113. Springer.

BILGER, R. W. 1989 Turbulent diffusion flames. *Ann. Rev. Fluid Mech.* **21**, 101–135.

CHAMEIDES, W. L. & STEDMAN, D. H. 1977 Tropospheric ozone: coupling transport and photo chemistry. *J. Geophys. Res.* **82**, 1787–1794.

CORRSIN, S. 1961 The reactant concentration spectrum in turbulent mixing with a first order reaction. *J Fluid Mech.* **11**, 407–416.

CORRSIN, S. 1964 Further consideration of Onsager's cascade model for turbulent spectra. *Phys. Fluids* **7**, 1156–1159.

CORRSIN, S. 1974 Limitations of gradient transport models in random walk and in turbulence. *Adv. Geophys.* **18**A, 25–60.

DONALDSON, C. DU P. & HILST, G. R. 1972 Effect of inhomogeneous mixing on atmospheric photo chemical reactions. *Environ. Sci. Technol.* **6**, 812–816.

DURBIN, P. A. 1980 A stochastic model of two-particle dispersion and concentration fluctuations in homogeneous turbulence. *J Fluid Mech.* **100**, 279–302.

GIBSON, M. M. JONES, W. P. & KANELLOPOULOS, V. E. 1989 Turbulent temperature mixing layer; Measurement and modelling. In *Turbulent Shear Flows 6* (ed. J.-C. Andre, J. Cousteix, F. Durst, B. Launder, F. Schmidt & J. Whitelaw), pp. 119–128. Springer.

HILL, J. C. 1976 Homogeneous turbulent mixing with chemical reaction. *Ann. Rev. Fluid Mech.* **8**, 135–161.

HINZE, J. O. 1975 Turbulence, 2nd edn. McGraw-Hill.

HSIEH, T.-H. J. & O'BRIEN, E. E. 1976 Prediction of single point concentration statistics in a chemically-reactive, turbulent, grid flow. *Combust. Sci. Technol.* **46**, 267–287.

JONES, W. P. & LAUNDER, B. E. 1972 The prediction of laminarization with a two-equation model of turbulence. *Intl J. Heat Mass Transfer* **15**, 301–314.

KEFFER, J. F., OLSEN, G. J. & KAWALL, J. G. 1977 Intermittency in a thermal mixing layer. *J Fluid Mech.* **79**, 596–607.

LAMB, R. G. 1976 Turbulent diffusion and air pollution. In *3rd Symp. on Atmosphere, Rayleigh, NC.*

LARUE, J. C. & LIBBY, P. A. 1981 Thermal mixing layer downstream of a half-heated turbulence grid. *Phys. Fluids* **24**, 597–603.

LARUE, J. C., LIBBY, P. A. & SESHADRI, D. V. R. 1981 Further results on the thermal mixing layer downstream of a turbulence grid. *Phys. Fluids* **24**, 1927–1933.

LAUNDER, B. E. 1976 Heat and mass transport. In *Turbulence* (ed. P. Bradshaw), p. 268. Springer.

LIBBY, P. A. 1975 Diffusion of heat downstream of a turbulence grid. *Acta Astronautica* **2**, 867–878.

LIBBY, P. A. & BRAY, K. N. C. 1981 Countergradient diffusion in pre-mixed flames. *AIAA J.* **19**, 205–213.

LIBBY, P. A. & WILLIAMS, F. A. (EDS) 1980 *Turbulent Reacting Flows.* Springer.

LIN, C.-H. & O'BRIEN, E. E. 1974 Turbulent shear flow mixing and rapid chemical reactions: an analogy. *J Fluid Mech.* **64**, 195–206.

LUMLEY, J. L. 1986 Evolution of a non-self-preserving thermal mixing layer. *Phys. Fluids* **29**, 3976–3981.

MA, B.-K. & WARHAFT, Z. 1986 Some aspects of the thermal mixing layer in grid turbulence. *Phys. Fluids* **29**, 3114–3120.

MANSOUR, M. S., BILGER, R. W. & DIBBLE, R. W. 1989 Spatial resolution in laser-based scalar measurements. *Tenth Australasian Fluid Mechanics Conf., University of Melbourne*, pp. 1.33–1.36.

MOSS, J. B. 1980 Simultaneous measurements of concentration and velocity in an open turbulent flame. *Combust. Sci. Technol.* **22**, 119–129.

MUDFORD, N. R. & BILGER, R. W. 1983 A facility for the study of nonequilibrium chemistry in an isothermal turbulent flow. In *Eighth Australasian Fluid Mechanics Conf., University of Newcastle, NSW*, pp. 7C.9–7C.12.

MUDFORD, N. R. & BILGER, R. W. 1985 Examination of closure models for mean chemical reaction using experimental data for an isothermal turbulent reacting flow. In *20th Symp. (Intl) on Combustion*, pp. 387–394. The Combustion Institute.

MUDFORD, N. R., BILGER, R. W. & IBRAHIM, S. S. 1991 Chemistry in a turbulent mixing flow from two opposed jets, to be published.

SAETRAN, L. R., HONNERY, D. R., STÅRNER, S. H. & BILGER, R. W. 1989 Scalar mixing layer in grid turbulence with transport of passive and reactive species. In *Turbulent Shear Flows 6* (ed. J.-C. Andre, J. Costeix, F. Durst, B. Launder, F. Schmidt & J. Whitelaw), pp. 109–118. Springer.

SEINFELD, J. H. 1985 *Air Pollution.* McGraw-Hill.

STEFFENSON, D. M. & STEDMAN, D. H. 1974 Optimization of the operating parameters of chemiluminescent nitric oxide detectors. *Analyt. Chem.* **46**, 1704–1709.

TENNEKES, H. & LUMLEY, J. L. 1972 *A First Course in Turbulence.* MIT Press.

TOOR, H. L. 1969 Turbulent mixing of two species with and without chemical reaction. *Indust. Engng Chem. Fund.* **8**, 655–659.

WARHAFT, Z. & LUMLEY, J. L. 1978 An experimental study of the decay of temperature fluctuations in grid generated turbulence. *J Fluid Mech.* **88**, 659–684.

WATT, W. E. & BAINES, W. D. 1973 Turbulent temperature mixing layer. *J. Hydraul. Res.* **11**, 157.

WU, M.-Z. & O'BRIEN, E. E. 1982 Prediction of single point temperature statistics in a half-heated grid flow. *Combust. Sci. Technol.* **29**, 53–66.

YIP, B. & LONG, M. B. 1986 Instantaneous planar measurement of the complete three-dimensional scalar gradient in a turbulent jet. *Opt. Lett.* **11**, 64–67.